ANALYTICAL CALCULATION OF INVARIANT DISTRIBUTIONS ON STRANGE ATTRACTORS

by

Kwok Yeung Tsang and M. A. Lieberman

Memorandum No. UCB/ERL M83/19

31 March 1983

ELECTRONICS RESEARCH LABORATORY

College of Engineering
University of California, Berkeley
94720

ANALYTICAL CALCULATION OF INVARIANT DISTRIBUTIONS ON STRANGE ATTRACTORS

by

Kwok Yeung Tsang and M.A. Lieberman

Department of Electrical Engineering and Computer Sciences
and the Electronics Research Laboratory
University of California, Berkeley, California 94720

ABSTRACT

We obtain analytically by an iterative procedure the equilibrium invariant distribution for a class of strange attractors found in two-dimensional perturbed twist maps. The zeroth order (phase-averaged) distribution is found by solving the appropriate Fokker-Planck equation. Repeated iterations over the map yield the higher order distributions that reveal successively finer structures. We develop a quantitative method to compare the maps thus obtained with the maps computed numerically. Using this method, the analytical theory has been verified for the dissipative Fermi, Zaslavskii and quadratic Chirikov maps, to the order that the numerical results can be obtained.

I. INTRODUCTION

It is well-known [1-3] that the steady state motion for a dissipative dynamical system may lie on a subset of phase space called a strange attractor. A strange attractor has the geometric structure of a Cantor set and therefore exhibits rescaling invariance; i.e., similar structures appear on even finer spatial scales. The motion on a strange attractor is mixing and ergodic.

For ergodic motion, we may replace the time average by a space average over the equilibrium invariant distribution on the ergodic subset in calculating the steady state value of a physical observable [4]. For a Hamiltonian system, the invariant distribution on any ergodic subset is trivially a constant on the constant energy surface. For a dissipative system, however, the equilibrium invariant distribution is not known a priori and must be found for each attractor of interest.

Our aim here is to present an approximate analytical approach for determining the structure of a strange attractor. This approach does not indicate whether a strange attractor exists in a given system. However, if the existence of the attractor is known, we can use the methods developed here to obtain approximately the equilibrium invariant distribution. Once the distribution is known, the expected value of an observable may be found by integrating over the distribution. For example, we may determine the average energy of an ensemble of stochastically heated particles whose dynamics are described by a dissipative map. Higher order moments and other quantities such as the Liapunov exponents can also be found.

The analysis is developed for a two-dimensional, invertible, perturbed twist map. The unperturbed map is assumed to be defined in terms

of the action-angle variables for an integrable Hamiltonian system. The perturbation is assumed to both destroy the integrability and to introduce dissipation. The basic assumption in the analysis is that the equilibrium invariant distribution, averaged over the unperturbed angle variable, can be determined from a Fokker-Planck equation in the action alone. Successively better approximations to the invariant distribution are then found by repeated iteration of the angle-averaged distribution over the map. Typically only a few iterations are required. The general method is developed in Section II.

In Section III, the dissipative Fermi map for a ball bouncing between a fixed inelastic wall and an oscillating elastic wall is introduced. This map serves to model a wide class of stochastic heating problems and is used to illustrate the method in some detail. The numerical results for the Fermi and other dissipative maps can be compared with analytical results not only qualitatively, but also quantitatively. In Section IV a quantitative comparison method is developed and applied to the Fermi map. In Section V two additional maps are introduced and used to illustrate other features and limitations of the theory.

II. THEORY

We consider an invertible perturbed twist map

$$T\,\underset{\sim}{z}_n = \underset{\sim}{z}_{n+1} \tag{1}$$

where

$$\underset{\sim}{z}_n = (x_n, y_n),$$

of the form

$$y_{n+1} = y_n + \epsilon F(x_n, y_{n+1}) \tag{2}$$

$$x_{n+1} = x_n + A(y_{n+1}) + \epsilon G(x_n, y_{n+1}) \tag{3}$$

Here F and G are periodic in x with period 2π, and $\underset{\sim}{z} = (x,y)$ are the angle-action variables of the unperturbed ($\epsilon \equiv 0$) Hamiltonian system.

Now suppose that for some ϵ a strange attractor exists with a basin of attraction B. We seek to construct by successive approximations the equilibrium invariant distribution f(x,y) for the attractor. This distribution satisfies the conditions

$$f(x,y) = Tf(x,y) \quad , \tag{3}$$

$$\frac{1}{2\pi} \int_B f dx dy = 1 \quad . \tag{4}$$

Although there are many invariant distributions for an attractor, a particular one (the equilibrium distribution) is singled out by the fact that the time average over almost any orbit in B is equal to the ensemble average for this distribution.

The method proceeds from the coarse scaled features of f to the fine scaled. We begin by finding a phase-averaged invariant distribution $\bar{f}(y)$. To do this we assume that $\bar{f}(y,n)$ evolves with the "time" (iteration number) n as a Markov process in y alone

$$\bar{f}(y,n) = \int \bar{f}(y-\Delta y,0) P(y-\Delta y,n|\Delta y) d(\Delta y) \tag{5}$$

where $P(y,n|\Delta y)$ is the probability that an initial ensemble of phase space points at y suffers an increment Δy after a time n. We make the additional assumption that $n \gg 1$ and that $\Delta y \ll (f^{-1} df/dy)^{-1}$; i.e., there exists an n such that in terms of (2),

$$1 \ll n \ll \left(\frac{\epsilon F_{max}}{f} \frac{df}{dy}\right)^2 \quad . \tag{6}$$

Under these conditions (5) can be written in the form of a Fokker-Planck equation

$$\frac{\partial \bar{f}}{\partial n} = -\frac{\partial}{\partial y}(B\bar{f}) + \frac{1}{2}\frac{\partial^2}{\partial y^2}(D\bar{f}) \ , \tag{7}$$

where the friction coefficient is

$$B(y) = \frac{1}{n}\int \Delta y P(y,n|\Delta y)d\Delta y \tag{8}$$

and the diffusion coefficient is

$$D(y) = \frac{1}{n}\int (\Delta y)^2 P(y,n|\Delta y)d\Delta y \ . \tag{9}$$

If we make the random phase assumption, (8) and (9) become

$$B(y) = \frac{1}{2\pi}\int_0^{2\pi} dx(\Delta y) \tag{10}$$

$$D(y) = \frac{1}{2\pi}\int_0^{2\pi} dx(\Delta y)^2 \tag{11}$$

To obtain the usual quasilinear friction and diffusion coefficients, we use (2) to write

$$\Delta y(x,y) = \varepsilon F(x,y) \tag{12}$$

Substituting (12) into (10) and (11) yields the coefficients necessary to solve (7). Corrections to the quasilinear coefficients can also be found [5]. When the Fokker-Planck equation is a good approximation for the Markov process, then the equilibrium solution obtained from (7) is a good initial guess for the invariant distribution. In Sec. III, we shall see that distributions generated this way compare well with coarse scale averages of the numerical results.

To find better approximations for the equilibrium invariant distribution $f(x,y)$, we note that almost every initial distribution $f^{(0)}(x,y)$

within the basin B converges under repeated iteration of the map to f. We want to choose an $f^{(0)}$ with a simple form and a fast rate of convergence. The phase-averaged equilibrium distribution is certainly a good choice. We therefore take as our zeroth order approximation

$$f^{(0)}(x,y) = \bar{f}(y) \quad . \tag{13}$$

To find successively higher order approximations, we iterate (13) successively by the map. Letting $\underset{\sim}{z}' = (x',y')$ be the pre-image of $\underset{\sim}{z} = (x,y)$, the i and i+1 approximations are related by

$$f^{(i+1)}(x,y)dxdy = f^{(i)}(x',y')dx'dy'$$

which yields

$$f^{(i+1)}(\underset{\sim}{z}) = J\, f^{(i)}(\underset{\sim}{z}'(\underset{\sim}{z})) \quad , \tag{14}$$

where

$$J(T^{-1}\underset{\sim}{z}) = \left| \frac{\partial(x',y')}{\partial(x,y)} \right| \tag{15}$$

is the Jacobian of the inverse map

$$T^{-1}\underset{\sim}{z} = \underset{\sim}{z}'(\underset{\sim}{z}) \quad .$$

The first order invariant distribution is then

$$f^{(1)}(x,y) = J\, \bar{f}(y'(x,y)) \quad . \tag{16}$$

We can rewrite this in terms of T^{-1} as

$$f^{(1)}(\underset{\sim}{z}) = J(T^{-1}\underset{\sim}{z}) f^{(0)}(T^{-1}\underset{\sim}{z}) \quad . \tag{17}$$

By repeatedly applying (14) we obtain the nth order approximation

$$f^{(n)}(\underset{\sim}{z}) = f^{(0)}(T^{-n}\underset{\sim}{z}) \prod_{i=1}^{n} J(T^{-i}\underset{\sim}{z}) \ . \tag{18}$$

We will compare these successive analytical results with numerical results in the following sections.

III. THE FERMI MAP

A two-dimensional map can be used to model a realistic problem such as the cosmic ray acceleration mechanism proposed by Fermi [6], in which charged particles are accelerated by collisions with moving magnetic field structures. In the model, shown in Fig. 1, a ball bounces elastically back and forth between a fixed and an oscillating wall. The motion of the ball can be described by a two-dimensional area-preserving map and has been examined by a number of authors [7-10]. However, they have only considered the perfectly elastic case. Here we introduce the effect of energy dissipation during the ball's motion.

We adapt the simplified model [9] for Fermi acceleration in which the moving wall oscillates sinusoidally, $x_w(t) = a \cos \omega t$, and imparts momentum to the ball according to its velocity $\dot{x}_w$ without the wall changing its position in space. We introduce the dissipation by assuming that the ball suffers a fractional loss δ in velocity upon collision with the fixed wall. The map can then be written

$$\bar{u} = (1-\delta)u_n - \sin \psi_n \tag{19}$$

$$\bar{\psi} = \psi_n + \frac{2\pi M}{\bar{u}} \tag{20}$$

$$(\psi_{n+1}, u_{n+1}) = (\bar{\psi}, \bar{u}) \ \mathrm{sgn}\ \bar{u} \tag{21}$$

where $u_n = v_n/(2\omega a)$ is the normalized ball velocity and $\psi_n = \omega t_n$ is the

phase of the oscillating wall just before the nth collision of the ball with the oscillating wall, and $M = \ell/(16a)$ is the normalized distance between the two walls. The function $\operatorname{sgn} \bar{u} = \pm 1$ for $\bar{u} \gtrless 0$, and is introduced to maintain $u_{n+1} \geq 0$ for low velocities $u_n < (1-\delta)^{-1}$, as physically occurs in the exact model, while preserving the continuity of the map near $u = 0$. The phase space is compact since any $u > \delta^{-1}$ maps below itself in u. The Jacobian of the map is $1-\delta$, and thus the map is area-preserving for $\delta = 0$. The usual picture of Hamiltonian chaos then ensues, with intermingled regions of chaotic and regular motion (see [9] for details).

For $0 < \delta << 1$, the fixed points of the Hamiltonian map become attracting centers (sinks), the KAM surfaces of Hamiltonian map no longer exist, and the persistent chaotic motion associated with a strange attractor is absent. Although transient chaos is generally present in the separatrix regions surrounding the sinks, the motion ultimately becomes periodic. Focusing on the case $M = 100$, numerical computations show that periodic motion on a simple attractor is found for $0 < \delta < 0.02$, even for values of δ as small as 10^{-6}. The complete destruction of persistent chaos when a very small dissipation is added to a near-integrable Hamiltonian system is typical and probably generic behavior.

For $M = 100$, numerical computations strongly suggest that a strange attractor exists for $0.03 < \delta < 0.3$, although the existence of small gaps within this range where the motion is periodic cannot be excluded. Values of $\delta > 0.3$ were not explored. A typical case is $\delta = 0.1$. Figure 2a shows the (ψ, u) surface of section in the range $4 \leq u \leq 6$ after 500,000 iterations of a single initial condition. The leaved structure of the attractor is quite evident. Figure 2b shows the expanded region $4.4 \leq u \leq 4.8$; we now see finer structures within the leaves. Here the expanded region has

been divided into 100 intervals along u and 100 intervals along ψ, forming 10,000 cells. The map is iterated 3×10^6 times for a single initial condition, and the number inside each cell (not readily seen) is a logarithmic measure of the number of occupations.

When the number of occupations per cell is summed over the phases ψ at a fixed u, the phase-averaged invariant distribution $\bar{f}(u)$ is obtained numerically. To determine $\bar{f}$ analytically, we use the phase-averaged Fokker-Planck equation (7). From (19),

$$\Delta u(\psi) = -\delta u - \sin \psi \quad . \tag{22}$$

Inserting (22) in (10) and (11), we find the dynamical friction

$$B = \frac{1}{2\pi} \int_0^{2\pi} (\Delta u) d\psi = -\delta u \tag{23}$$

and the diffusion coefficient

$$D = \frac{1}{2\pi} \int_0^{2\pi} (\Delta u)^2 d\psi = \frac{1}{2} + \delta^2 u^2 \quad . \tag{24}$$

In the steady state and with no net flux of particles, the Fokker-Planck equation becomes

$$-B\bar{f} + \frac{1}{2} \frac{d}{du} (D\bar{f}) = 0 \quad . \tag{25}$$

Typically $\delta^2 u^2 << \frac{1}{2}$, so we drop the second item in (24), insert (23) and (24) into (25), and integrate to obtain

$$\bar{f}(u) = \left(\frac{8\delta}{\pi}\right)^{1/2} \exp(-2\delta u^2) \quad . \tag{26}$$

The integration constant has been found from the requirement that

$$\int_0^{\infty} \bar{f}(u) du = 1 \quad .$$

In Fig. 3, we compare this analytic expression (solid line) with the numerical results for $\delta = 0.1$ and various values of M in the range 20-500. The numerical points all lie along the same straight line, independent of M. The theory and numerical calculations are in good agreement at low velocities, but there is some deviation at higher velocities. This is understandable since from inequality (6), the Fokker-Planck description is strictly valid only provided

$$\left| \frac{1}{\bar{f}} \frac{d\bar{f}}{du} \right|^{-1} \gtrsim 1 \ .$$

Using (26), we obtain the condition for validity $u \lesssim (4\delta)^{-1}$. However, we note from Fig. 3 that the Fokker-Planck solution well approximates the phase-averaged numerical results for u's considerably greater than $(4\delta)^{-1} = 2.5$. We therefore use (26) in (13) to determine the zeroth order invariant distribution $f^{(0)}(\psi,u) = \bar{f}(u)$.

To find the first order distribution, we use (16) with $J = (1-\delta)^{-1}$ and, inverting the Fermi map, we obtain

$$f^{(1)}(\bar{\psi},\bar{u}) = \frac{1}{1-\delta} \left(\frac{8\delta}{\pi}\right)^{1/2} \exp\left\{ - \frac{2\delta}{(1-\delta)^2} \left[\bar{u} + \sin\left(\bar{\psi} - \frac{2\pi M}{\bar{u}}\right) \right]^2 \right\} . \qquad (27)$$

If we introduce the inverse of the Fermi map

$$T^{-1}(\psi,u) = \left(\psi - \frac{2\pi M}{u} \ , \ \frac{u + \sin\left(\psi - \frac{2\pi M}{u}\right)}{1 - \delta} \right) , \qquad (28)$$

then using (16), we can rewrite (27) as

$$f^{(1)}(\psi,u) = (1-\delta)^{-1} \ f^{(0)}(T^{-1}(\psi,u)) \ .$$

Since J is a constant independent of (ψ,u), the nth order distribution

is found from (18) to be

$$f^n(\psi,u) = (1-\delta)^{-n}\bar{f}^{(0)}(T^{-n}(\psi,u)) \ . \qquad (29)$$

To compare (27) with the numerically calculated invariant distribution $f(\psi,u)$, we plot in Fig. 4a the expected occupation numbers using $f^{(1)}$, in the same expanded region of the surface of section as for the numerical calculation of f in Fig. 2b. The same number of total occupations (3×10^6) and the same logarithmic measure for the number of occupations in each of the 100×100 cells are used. The band structure seen in the magnified image of $f^{(1)}$ corresponds closely to the numerically determined bands seen in Fig. 2b.

To see a still closer correspondence between theory and numerical calculation, we plot the higher order expressions $f^{(2)}$, $f^{(3)}$ and $f^{(4)}$ in Fig. 4b, c and d. We see that $f^{(1)}$, $f^{(2)}$ and perhaps $f^{(3)}$ show successively better agreement with the numerical calculation.

In determining the average value of $f_j^{(n)}$ in cell j from the theory (29), it is not sufficient to map just the midpoint of the cell backward n times to obtain $\bar{f}$. In principle we should map the entire set of points within the cell backward and determine $\bar{f}$ as an average over this set. In practice it is necessary to choose a sufficient number of points within each cell to average over the fine-scaled structures formed by n mapping iterations. For $f^{(1)}$, $f^{(2)}$, $f^{(3)}$, and $f^{(4)}$, we use 1, 1, 81 and 121 points respectively, uniformly distributed over each cell, and have verified that $f_j^{(n)}$ for all j is unchanged when additional points are used.

Theoretically, the higher we go in the order, the better the agreement with numerical calculation we should get. However, it is not persuasive to say that Figs. 4a,b,c,d are in progressively good agreement

with the numerical calculation. To claim that one theoretical map appears in closer agreement with the numerically generated map than another is subjective. Furthermore, the agreement between maps having fine structures is restricted by the size of the cells. This explains why $f^{(4)}$ doesn't seem much better than $f^{(2)}$, as the fourth order structures are smaller than the chosen cell size.

IV. QUANTITATIVE COMPARISON OF MAPS

To compare maps quantitatively, we must introduce a measure E^2 for the resemblance between two maps f and g, each having N occupations in a domain which has been partitioned into K cells. We use the mean square hyperbolic deviation*

$$E^2 = \frac{4}{N} \sum_{j=1}^{K} (\sqrt{f_j} - \sqrt{g_j})^2 , \tag{30}$$

where $f_j \geq 0$ and $g_j \geq 0$ are the number of occupations in cell j, with

$$\sum_{j=1}^{K} f_j = \sum_{j=1}^{K} g_j = N .$$

We note that E^2 has the following desirable properties: It is symmetric in f and g. It is defined even if some f_j's or g_j's are zero. It is unchanged if the normalization N is doubled, because each f_j and g_j is also doubled. It is unchanged if the number of cells is doubled, because each f_j and g_j is halved. Putting $N = \mu K$ in (30), with μ the mean occupation

*The hyperbolic mean of two quantities X and Y is defined as $2|X^{-1} + Y^{-1}|^{-1}$. The deviation of g_j from f_j is $|f_j - g_j|/\sqrt{f_j}$; the deviation of f_j from g_j is $|f_j - g_j|/\sqrt{g_j}$. The hyperbolic mean of these two deviations is $2|\sqrt{f_j} - \sqrt{g_j}|$.

number, we see that E represents the average (rms) hyperbolic mean number of standard deviations $\sqrt{\mu}$ by which f and g differ.

The comparison of numerically generated maps is limited by random fluctuations. If we compare the uniform map $f_j = \mu$ with the random map $g_j = \{k\}$ having a Poisson distribution

$$p_k = \frac{\mu^k e^{-\mu}}{k!}$$

then we obtain

$$E_R^2(\mu) = \frac{4}{\mu} \sum_{k=0}^{\infty} p_k (\sqrt{\mu} - \sqrt{k})^2 \tag{31a}$$

For $\mu << 1$, $E_R^2 = 8$, while for $\mu >> 1$, $E_R^2 = \mu^{-1}$. Similarly, we can compare two random maps each having Poisson distribution to obtain

$$E_{RR}^2(\mu) = \frac{4}{\mu} \sum_{k=0}^{\infty} \sum_{\ell=0}^{\infty} p_k p_\ell \, (\sqrt{k} - \sqrt{\ell})^2 \tag{31b}$$

For $\mu << 1$, $E_{RR}^2 = 8$, while for $\mu >> 1$, $E_R^2 = 2\mu^{-1}$. In Fig. 5, E_R^2 and E_{RR}^2 are plotted versus μ.

We use E^2 to measure the resemblance between two maps. The maps are exactly the same if $E^2 = 0$. The maps do not resemble each other if $E^2 >> 1$. The maps resemble each other to within one standard deviation if $E^2 = 1$.

An experiment (iteration of a map) generates a Poisson distribution of occupation numbers. Therefore, if a theory and an experiment agree exactly (except that the experiment is corrupted by noise), then the best agreement we can expect is $E^2 \approx E_R^2$. Similarly if two experiments agree exactly (but both are corrupted by noise), we expect to find $E^2 \approx E_{RR}^2$.

It is not reasonable to test two maps for resemblance unless we can expect $E^2 \lesssim 1$. We see from Fig. 5 that to test for agreement between theory and experiment we require $\mu \gtrsim 2$. Similarly, from Fig. 5, we require $\mu \gtrsim 3$ to test whether two experiments resemble each other. These requirements set limits on determining whether fine structures of maps generated by numerical computation resemble each other. The maximum practical storage size ($\propto K$) and time limit ($\propto N$) set the ratio $\mu = N/K$.

Using E^2 as a measure we now examine the validity of the theory. Table 1 gives the values of E^2 obtained when the theoretical maps $f^{(0)}$ through $f^{(4)}$ are compared with a typical numerical map. The numbers of points per cell needed to accurately determine the theoretical occupation numbers were 1, 1, 1, 81, 121 for $f^{(0)}$ through $f^{(4)}$ respectively. Two comparisons for different regions of u are shown. The first column gives E^2 for $4.4 \leq u \leq 4.8$, when the theoretical maps in Fig. 4a-d are compared with the numerical result in Fig. 2b. For these data, $\mu = 0.94$, and from Fig. 5, the best we may expect if the theory and numerical result resemble each other is $E_R^2 \approx 1.92$. (We would prefer μ to be larger for this case.) We see that E^2 falls from 1.94 for $f^{(0)}$ to 1.2 for $f^{(4)}$, and that the higher-order theoretical maps closely resemble the numerical map.

A second comparison is given for $2.8 \leq u \leq 3.2$ in column 2. Here $\mu = 3.8$ and from Fig. 5 we expect $E_R^2 \approx 0.33$ if the theory and numerical results resemble each other. We see that E^2 falls from 1.37 for $f^{(0)}$ to 0.38 for $f^{(3)}$. We conclude from the data in both regions of u that theory and numerical results agree.

We have also examined the sensitivity of the agreement between theory and experiment to the choice of $f^{(0)}$ as the phase-averaged distri-

bution obtained from the Fokker-Planck equation. Instead of (26), we choose

$$\bar{f}(u) = \left(\frac{4\gamma\delta}{\pi}\right)^{1/2} \exp(-\gamma\delta u^2) \tag{32}$$

and use this in (29) to determine $f^{(2)}$. We then calculate E^2 for various values of the parameter γ. In Fig. 6, E^2 is plotted versus γ for the two regions $2.8 \leq u \leq 3.2$ and $4.4 \leq u \leq 4.8$ described previously. We see that in both cases the maximum resemblance (minimum E^2) occurs near $\gamma = 2$. This indicates that the Fokker-Planck solution is the proper initial choice for $\bar{f}$.

V. OTHER MAPS

We have seen that the theory agrees well with numerical results for the Fermi map. We now examine two other maps to determine its applicability and limitations.

A two-dimensional mapping can be used to model the motion of charged particles in a field of electrostatic waves [11]. The mapping can be reduced to a simple form called the Zaslavskii map [12,13],

$$\begin{aligned} x_n &= x_{n-1} + y_n \\ y_n &= (1-\delta)y_{n-1} + k \sin 2\pi x_{n-1} \end{aligned} \tag{33}$$

where x (taken modulo 1) is the displacement and y is the velocity of a particle; k is proportional to the wave amplitude, and δ is a frictional drag coefficient. For small δ the phase-averaged distribution is found from the Fokker-Planck equation to be

$$\bar{f}(y) = \left(\frac{2\delta}{\pi}\right)^{1/2} \exp(-2\delta y^2/k^2) \ . \tag{34}$$

From (6) we expect this to be valid for $k \gtrsim 4\delta y$. To compare this result with a numerical calculation of $\bar{f}$ we choose $k = 5$ and $\delta = 0.1$. Numerically we find that a strange attractor exists. In Fig. 7 the theory is compared with the numerical result obtained from 10^6 iterations of a single initial condition. The agreement is good even for y's considerably larger than $k/(4\delta)$.

If we enlarge a portion of the numerically generated map, we see structures inside the attractor. Figure 8a shows 23641 occupations in the region $0 \leq x \leq 1$, $13 \leq y < 15$ for a single initial condition.

Applying the method described in Sec. II, we use (34) for the initial guess $f^{(0)}$ and determine the higher order distributions $f^{(1)}$, $f^{(2)}$ and $f^{(3)}$. These are shown in Fig. 8b,c and d respectively for the same number of occupations as for the numerical map in Fig. 8a. The increasing resemblance of the higher order maps to the numerical map is apparent. Quantitatively we find the results shown in column 3 of Table 1. E^2 falls from .88 for $f^{(1)}$ to .58 for $f^{(3)}$. The latter is close to the expected value $E_R^2 \approx 0.64$, yielding quantitative agreement.

To study a case where the theory breaks down we choose $k = 1.4$ and $\delta = 0.9$. A strange attractor is found numerically for these parameters. However, inequality (6) is not satisfied for the typical y's found in this case. Thus we do not expect the Fokker-Planck solution (34) to accurately represent the numerically determined phase-averaged distribution. The analytical and numerical distributions are compared in Fig. 9. The disagreement is apparent and it would seem better to determine the initial guess $f^{(0)}$ by direct solution of (5) or in some other manner. Nevertheless, the Fokker-Planck solution has roughly the same rms deviation in y as the numerical distribution. If we use the Fokker-Planck

solution for the initial guess and determine the higher order distributions, we still find fairly good agreement with numerical results. Figure 10a is the numerical result for 10^5 iterations of a single initial condition (shown as the cross). Figures 10b and 10c are the corresponding analytical results for the first two orders $f^{(1)}$ and $f^{(2)}$. We see that they closely resemble the numerical result. Figure 11a is an enlargement of the small boxed portion in Fig. 10a. Here we have chosen a single initial condition iterated 10^6 times, for a total of 37326 occupations of the map. In Fig. 10b we have chosen 10 initial conditions each iterated 10^5 times instead. The small deviation $E^2 \approx .08$ between these two maps suggests that the numerically calculated map is independent of the initial conditions chosen.

In Fig. 11c, $f^{(2)}$ is plotted using the Fokker-Planck initial guess for the same regions as the numerical plots in Fig. 11a and b. We see that the structures look similar. Thus the theory reproduces the shape of the numerical structures for this case, although E^2 obtained is somewhat larger than E_R^2 expected (see column 4 and 5 in Table 1). This is understandable because the zero-order distribution found from the Fokker-Planck equation is not such a good approximation to the numerically determined phase-averaged distribution (see Fig. 9).

We can continue to look at finer structures by going to higher order, thus demonstrating the rescaling invariance of the theory. In Fig. 12a, the boxed region in Fig. 11c is expanded by a factor of 77.5 in each direction, and $f^{(3)}$ is plotted. In Fig. 12b, the boxed region in Fig. 12a is expanded again by the same factor, and $f^{(4)}$ is plotted. The rescaling invariance of the theory is apparent.

The factor 77.5 was originally chosen heuristically to obtain the best agreement between the rescaled maps. We can understand the rescaling factor analytically by examining how a small line segment transforms.

In order n+1, the vertical line segment between two leaves at $(0,\Delta y_1)$ and $(0,-\Delta y_1)$ is transformed by the inverse map to the line segment $(-\Delta y_1,-\alpha\Delta y_1)$ to $(\Delta y_1,\alpha\Delta y_1)$, where

$$\alpha = \frac{2k\pi-1}{1-\delta} = 77.96 \quad .$$

The endpoints lie on the corresponding leaves in order n. Since the slope dy/dx of the leaves is approximately unity, the length of a vertical line segment between leaves in order n is a factor of $\alpha-1 \approx 76.96$ times the corresponding length in order n+1. If maps similar to Fig. 12a and 12b obtained numerically are desired, they would require roughly 10^9 and 10^{11} iterations of the map respectively! It is therefore not possible, using our computational resources, to compare these analytical maps with their corresponding numerical maps. However, if we compare each of these rescaled, high order analytical maps with the previous numerical map (Fig. 11a) displaying the second order structures, we get an E^2 comparable to that of the second order analytical map. (See column 5 in Table 1.) This verifies not only qualitatively, but also quantitatively, that the theory can reproduce the rescaling property of the strange attractor. We see that the analytical theory is capable of exhibiting the structures of a strange attractor that numerical iteration of the mapping can hardly reach.

As a final example we consider the Chirikov map [14,15] that models a nonlinear oscillator with p and x as action-angle variables:

$$\begin{aligned} \bar{p} &= \{p+k\cdot g(x) - \delta(p-\tfrac{1}{2})\} \ , \\ \bar{x} &= \{x+\bar{p} - \tfrac{1}{2}\} \quad , \end{aligned} \tag{35}$$

where braces denote the fractional part, which describes a periodic dependence (of unity period) in both angle and action. We consider the perturbation

$$g(x) = x^2 - x + 1/6 \quad . \tag{36}$$

Figure 13a shows the numerically calculated distribution for $k = 9.76$ and $\delta = 0.2$ using 10^5 iterations of a single initial condition. Because the action variable is taken modulo 1 in (35), it is not straightforward to calculate the phase-averaged distribution $\overline{f}$ from the Fokker-Planck equation. To estimate the variation of $\overline{f}$ over the unit interval we remove this mod function and solve the Fokker-Planck equation (7) in the extended action space $-\infty < p < \infty$, obtaining

$$\overline{f} \propto \exp[-180\delta(p - \tfrac{1}{2})^2/k^2] \tag{37}$$

For $k = 9.76$, $\delta = 0.2$, we find that $\overline{f}(0) = \overline{f}(1) \approx .91\overline{f}(\frac{1}{2})$; i.e., $\overline{f}$ does not vary much over $0 \leq p < 1$. We therefore use the uniform distribution $\overline{f} = 1$ as the zero order distribution $f^{(0)}$. Figures 13b,c and d show $f^{(1)}$, $f^{(2)}$ and $f^{(3)}$ using 1, 9 and 25 points per cell respectively, each iterated backwards to obtain the theoretical distributions. The last column in Table 1 gives E^2 for the comparison of $f^{(1)}$ through $f^{(4)}$ with the numerical map Fig. 13a. We see that E^2 drops from 0.6 for $f^{(1)}$ to 0.12 for $f^{(4)}$, the latter being close to the expected value $E_R^2 = 0.11$. Thus $f^{(4)}$ strongly resembles the numerical map.

VI. CONCLUSION

The approximate equilibrium invariant distribution on a strange attractor for a general, two-dimensional perturbed twist map has been determined analytically. The invariant distribution is found by

iterating a certain phase-averaged distribution over the map. This phase-averaged distribution is the stationary solution of the appropriate Fokker-Planck equation for the map. The number of iterations required depends on the size of the features of the invariant distribution that one wishes to resolve. Given present limits on speed and storage capacity for digital computers, five or six iterations are generally sufficient to resolve the finest features that can be observed by direct numerical iteration of a set of initial conditions over the map.

Three maps have been studied numerically: the dissipative Fermi map that is often used to model stochastic heating processes, the Zaslavskii map that often appears as a model for wave-particle interactions and for the beam-beam effect in high energy storage rings, and the quadratic Chirikov map that has been applied generally to the study of dissipative dynamics. For all three maps the numerically calculated invariant distributions are in qualitative (visual) agreement with the analytical distributions.

A method for quantitatively comparing the analytical and numerical distributions in the presence of statistical (Poisson) fluctuations in the latter has been introduced. Using this method, the mean square hyperbolic deviation between the two distributions is numerically calculated and tested for significance against the expected deviation due to statistical fluctuations alone. For all maps and phase space regions studied, the analytical and numerical distributions are found to agree quantitatively.

The extension of these results to perturbed twist maps having more than two dimensions seems relatively straightforward. We also note that the dynamics of perturbed integrable systems can generally be described in terms of a perturbed twist mapping on a surface of section. Thus the

Errata: Page 16: in line 7, Fig. 10a should read Fig. 10c.

in line 9, Fig. 10b should read Fig. 11b.

analytical method introduced here for determining the equilibrium invariant distribution on a strange attractor is expected to be applicable to a wide class of dissipative dynamical systems.

ACKNOWLEDGEMENT

Research sponsored by the Office of Naval Research Contract N00014-79-C-0674 and the National Science Foundation Grant ECS-8104561.

References

[1] R.H.G. Helleman, in Fundamental Problems in Statistical Mechanics, Vol. 5, E.G.D. Cohen (ed.), North Holland, Amsterdam, (1980), p. 165.

[2] R. Shaw, Z. Naturforsch. 36A (1981) 80.

[3] E. Ott, Rev. Mod. Phys. 53(1981) 655.

[4] A.J. Lichtenberg and M.A. Lieberman, Regular and Stochastic Motion, Springer-Verlag, New York (1982) 413.

[5] A.B. Rechester, M.N. Rosenbluth and R.B. White, Phys. Rev. A23 (1981) 2664.

[6] E. Fermi, Phys. Rev. 15 (1949) 1169.

[7] G.M. Zaslavskii and B.V. Chirikov, Soviet Physics Doklady 9 (1965) 989.

[8] A. Brahic, Astr. and Astrophys. 12 (1971) 98.

[9] M.A. Lieberman and A.J. Lichtenberg, Phys. Rev A5 (1972) 1852.

[10] A.J. Lichtenberg, M.A. Lieberman and R.H. Cohen, Physica 1D (1980) 291.

[11] R.V. Jensen and C.R. Oberman, Physica 4D (1982) 183.

[12] G.M. Zaslavskii, Phys. Lett. 69A (1978) 45.

[13] G.M. Zaslavskii and Kh.-R. Ya. Rachko, JETP 49 (1979) 1039.

[14] B.V. Chirikov and F.M. Izrailev, Colloques Internationaux du C.N.R.S., No. 229, Paris (1976) 409.

[15] B.V. Chirikov and F.M. Izrailev, Physica 2D (1981) 30.

TABLE 1. COMPARISON OF THEORY AND NUMERICAL RESULTS

Map		Fermi ($M = 100$, $\delta = 0.1$)		Zaslavskii ($k = 5$, $\delta = 0.1$)	Zaslavskii ($k = 1.4$, $\delta = 0.9$)		Chirikov ($k = 9.76$, $\delta = 0.2$)
region		$4.4 \leq u < 4.8$	$2.8 \leq u < 3.2$	$13 \leq y \leq 15$	$\|y\| \leq 2$	$\|y\| \leq .06$	$0 \leq p < 1$
μ		0.94	3.8	2.4	10	3.7	10
E_R^2		1.92	0.33	.64	.11	0.35	0.11
E^2	$f^{(0)}$	-	1.37	-	5.31	-	-
	$f^{(1)}$	1.94	0.42	.88	1.02	4.5	0.6
	$f^{(2)}$	1.13	0.38	.60	0.20	0.92	0.23
	$f^{(3)}$	1.20	0.38	.58	-	*0.92	0.14
	$f^{(4)}$	1.20	-	-	-	**0.98	0.12

*Rescaling $|y| \leq .000775$ to $|y| \leq .06$.

**Rescaling $|y| \leq .00001$ to $|y| \leq .06$.

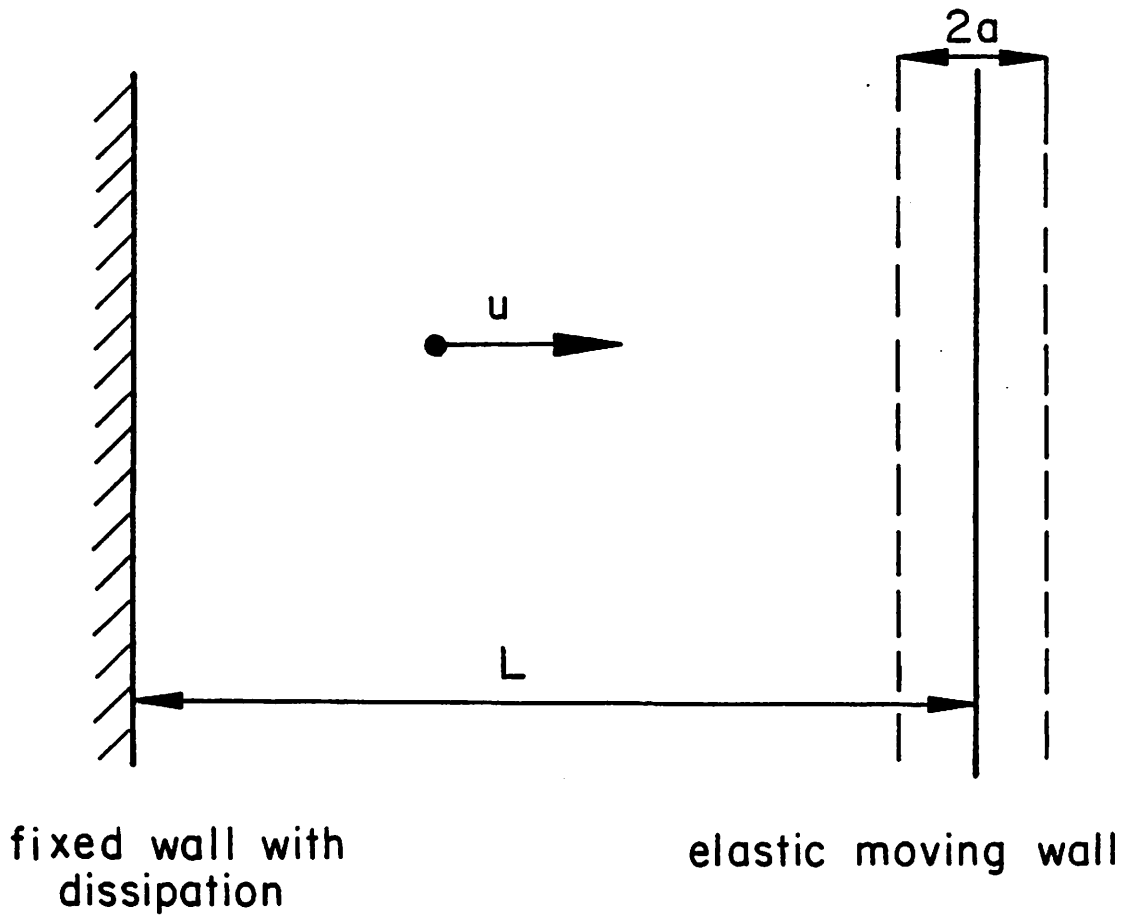

Fig. 1. One-dimensional dissipative Fermi problem.

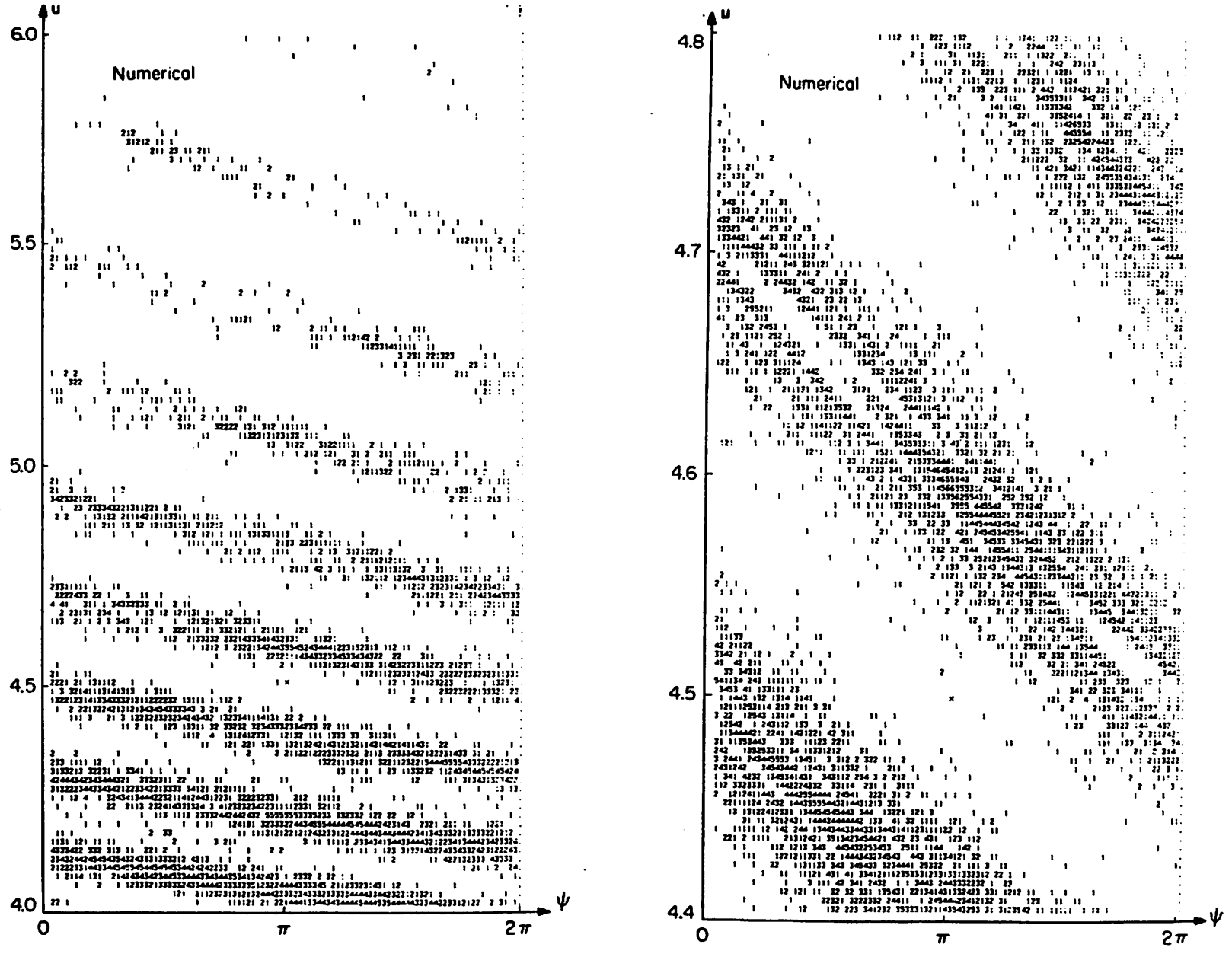

(a) (b)

Fig. 2. Phase space u-ψ for the Fermi map with M = 100 and δ = 0.1.

(a) One particle with 500,000 collisions, of which 5943 occupations appear in the range $4 \leq u < 6$.

(b) One particle with 3,000,000 collisions, of which 9382 occupations appear in the range $4.4 \leq u < 4.8$.

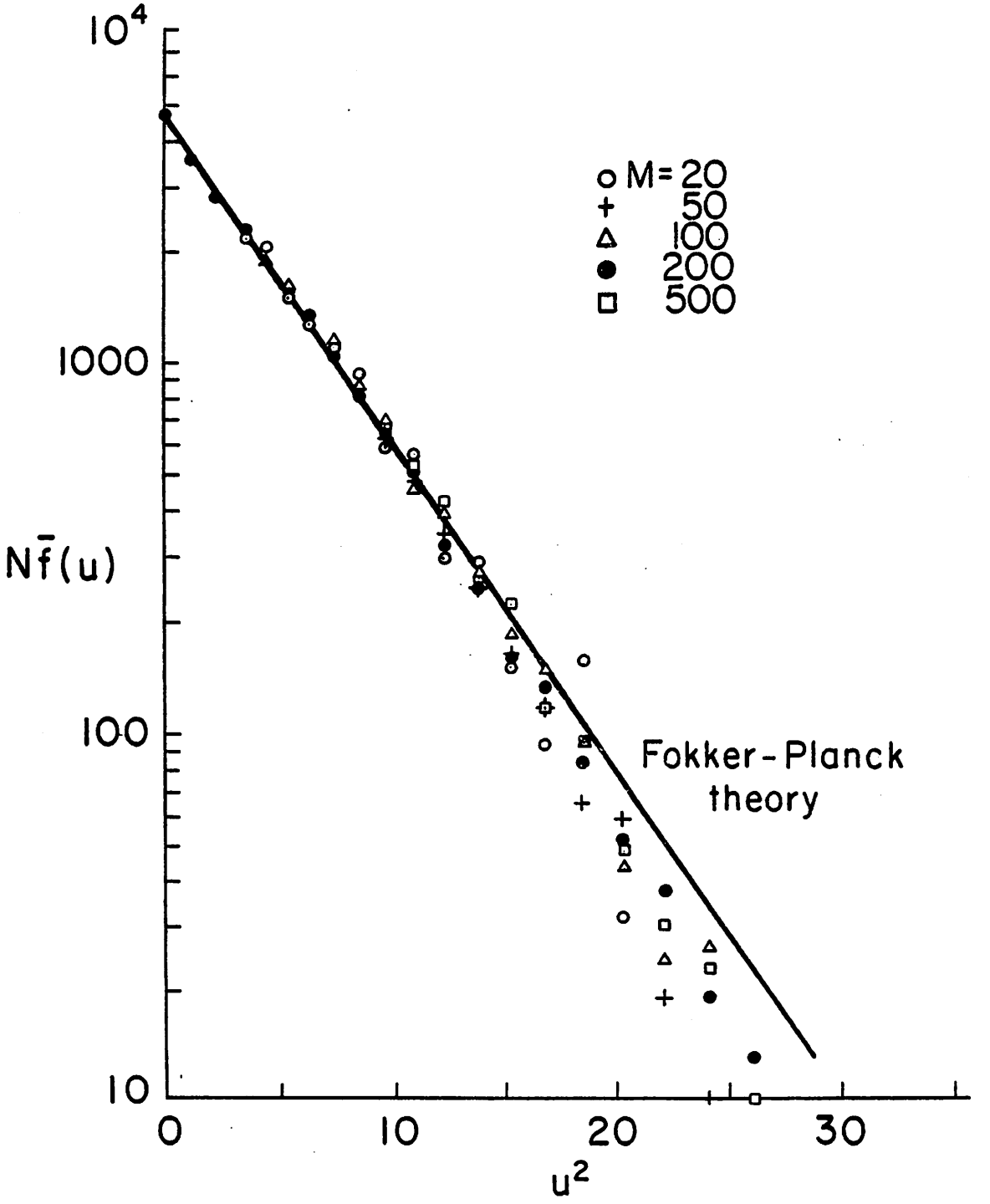

Fig. 3. Comparison of the numerically calculated phase-averaged invariant distribution with the Fokker-Planck solution $\bar{f}(u)$ for $\delta = 0.1$ and various values of M for the Fermi map.

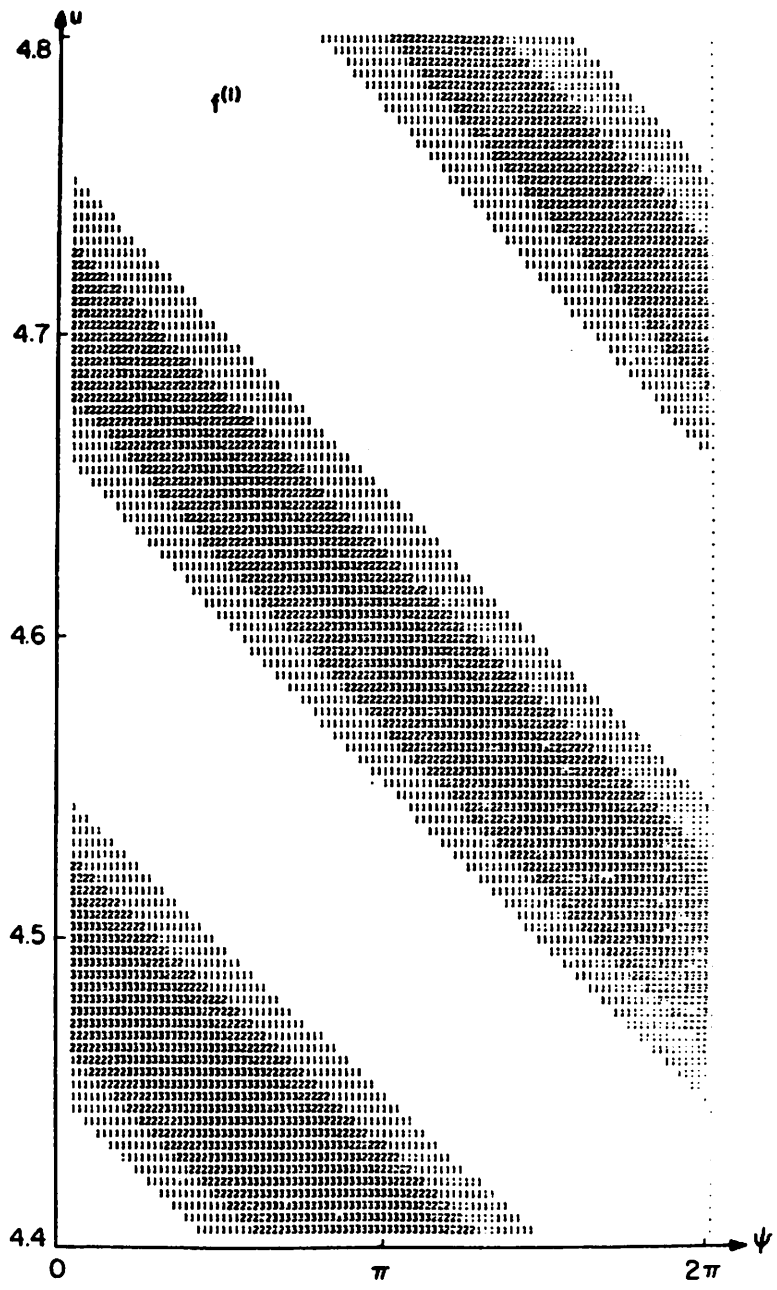

(a)

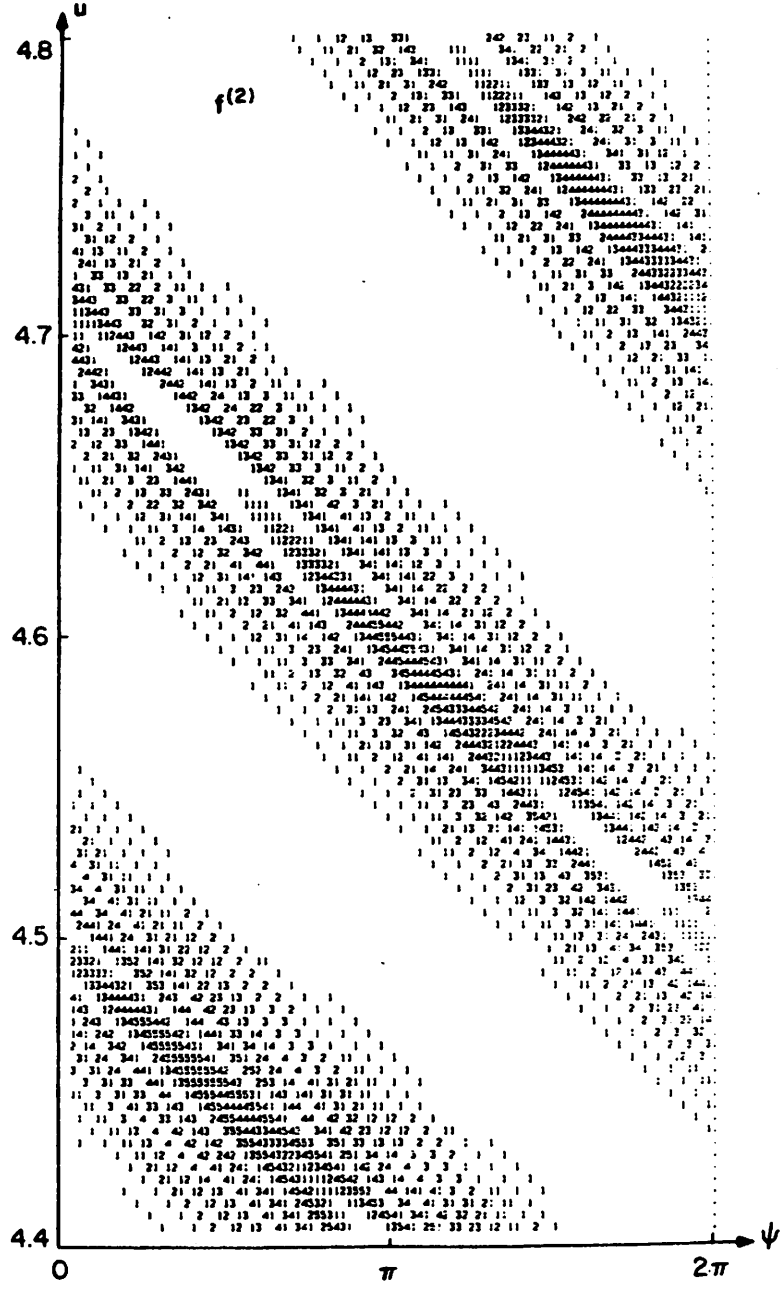

(b)

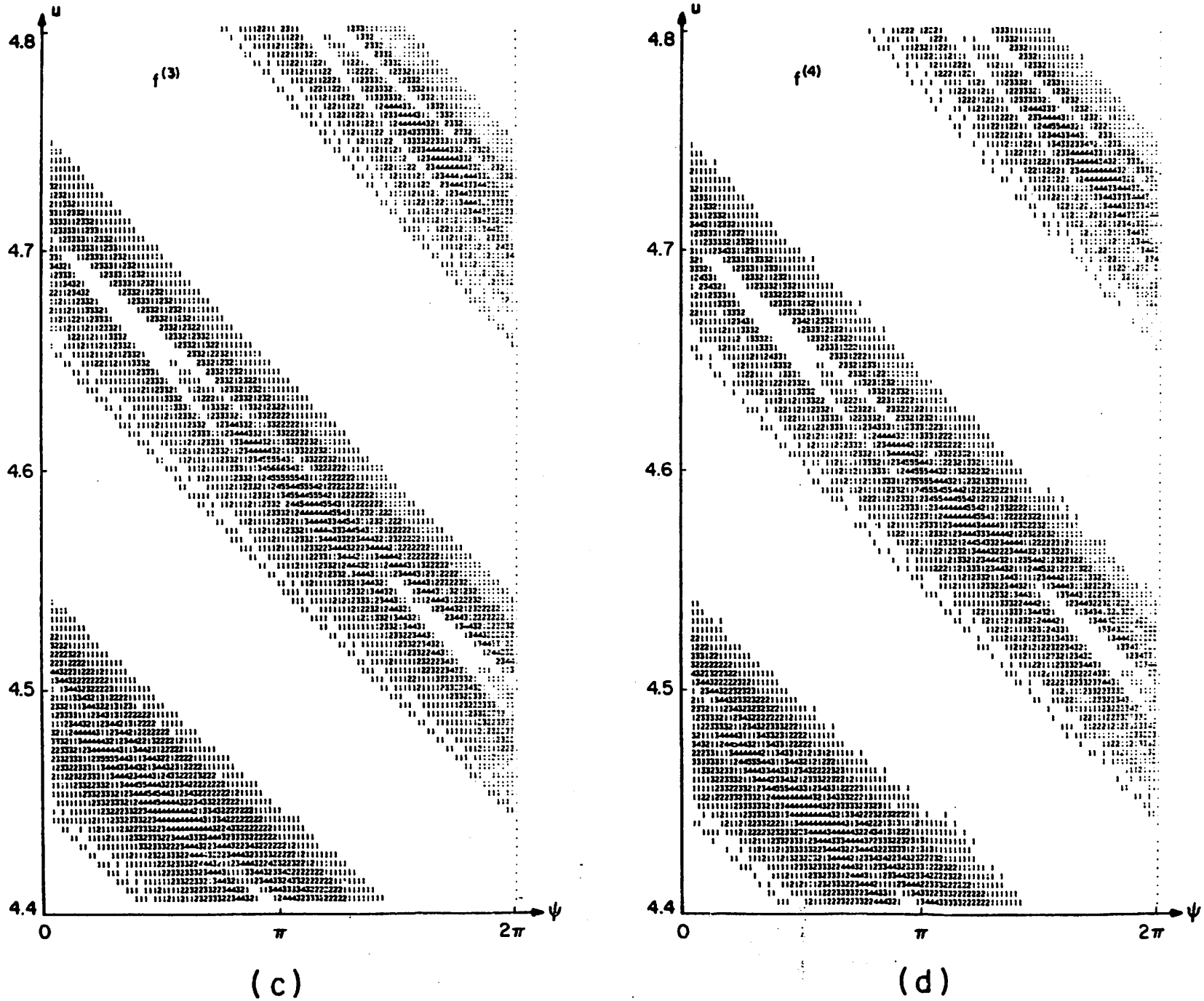

Fig. 4. Analytical calculation of the invariant distribution for dissipative Fermi acceleration; (a) First order result $f^{(1)}(\psi,u)$; (b) second order result $f^{(2)}(\psi,u)$; (c) third order result $f^{(3)}(\psi,u)$; (d) fourth order result $f^{(4)}(\psi,u)$. The functions are plotted by computer with the scales and effective number of iterations the same as for Fig. 2b.

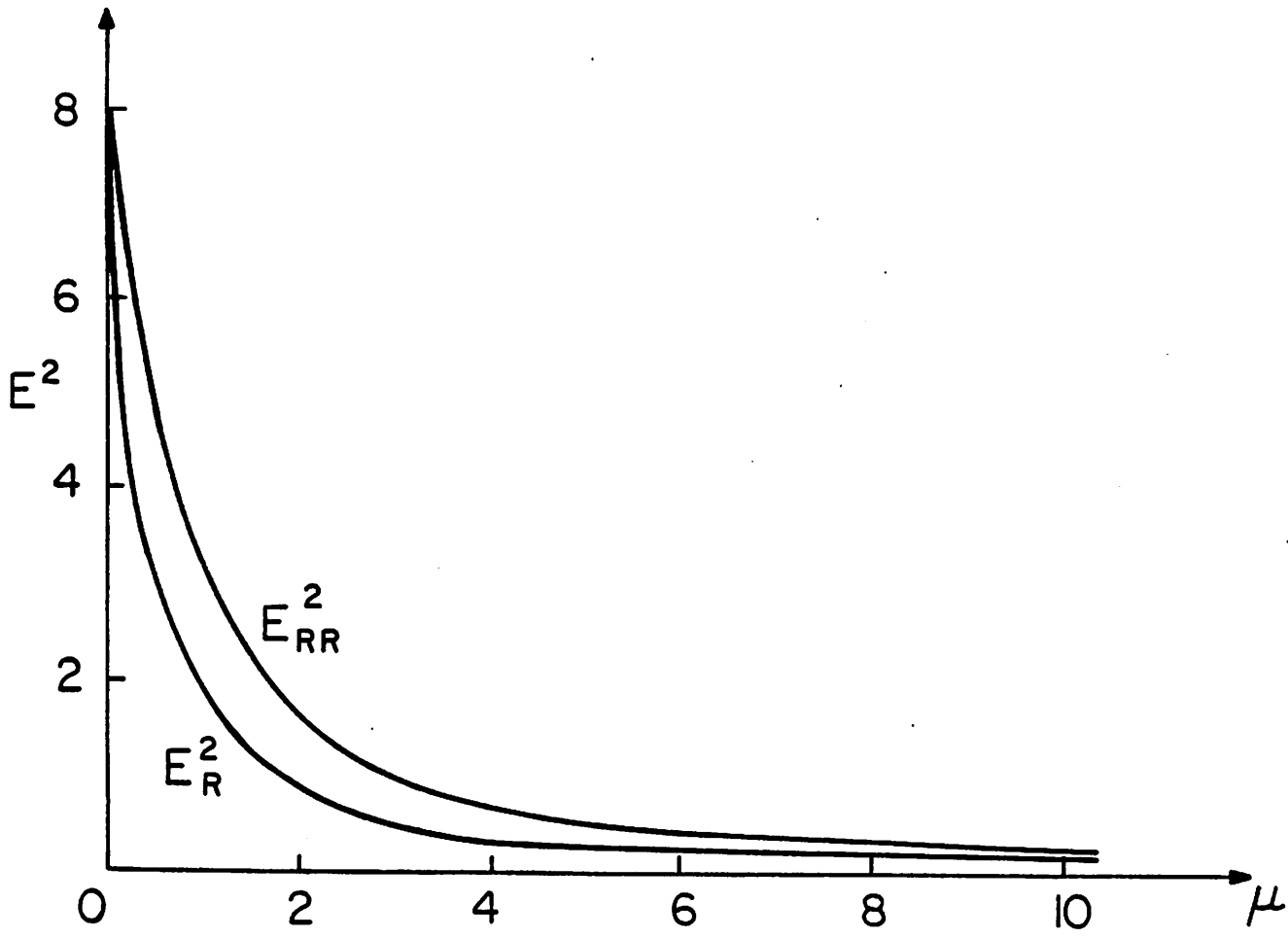

Fig. 5. Square of expected deviation E_R^2 between a uniform map and a random map having Poisson distribution; and square of expected deviation E_{RR}^2 between two random maps each having Poisson distribution, are plotted versus the mean occupation number μ.

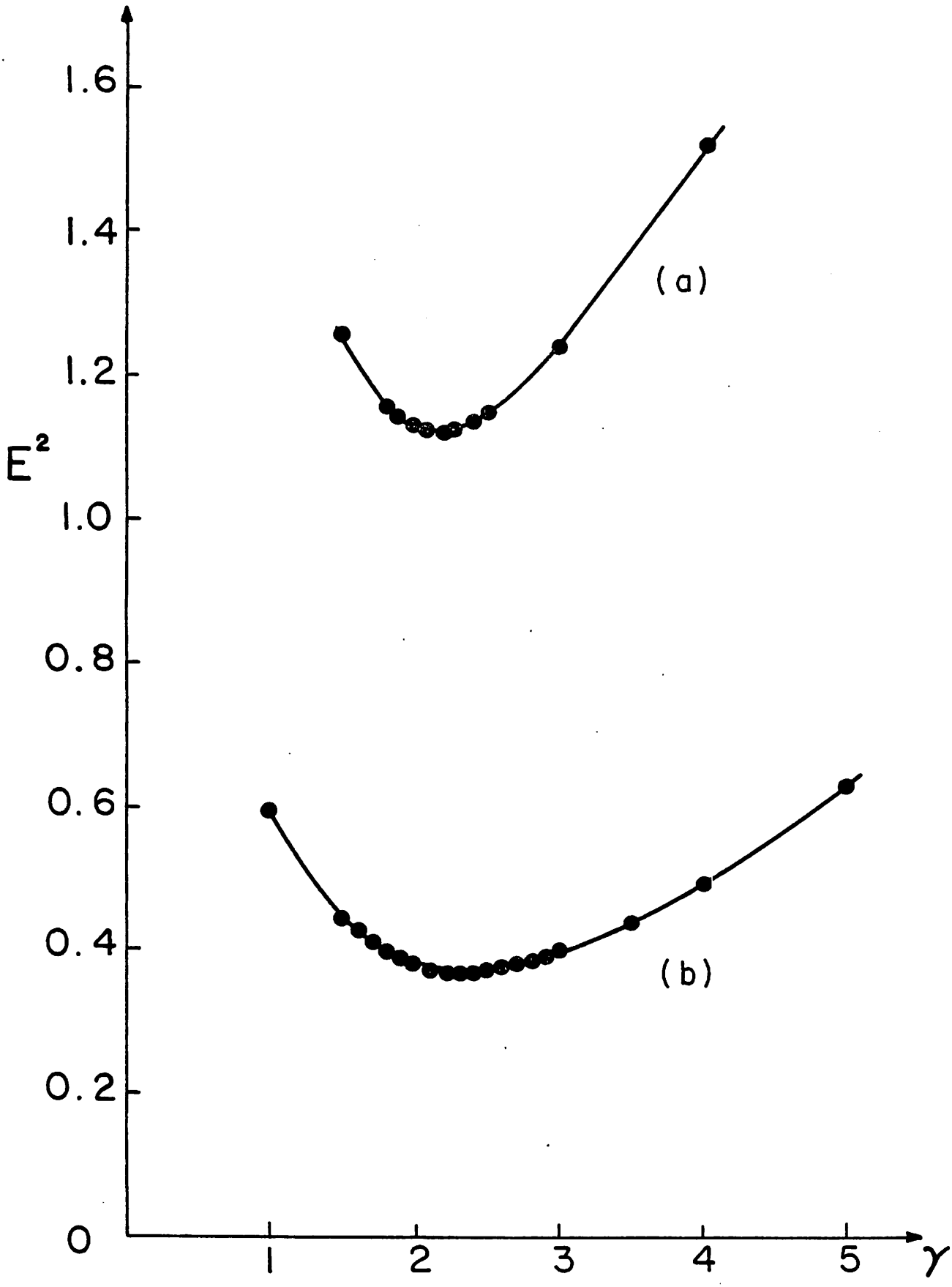

Fig. 6. Square of deviation E^2 for $f^{(2)}$ is plotted versus various values of the parameter γ [see Eq. (32) for the Fermi map]; (a) $4.4 \leq u \leq 4.8$ with $E_R^2 = 1.92$ and (b) $2.8 \leq u \leq 3.2$ with $E_R^2 = 0.33$.

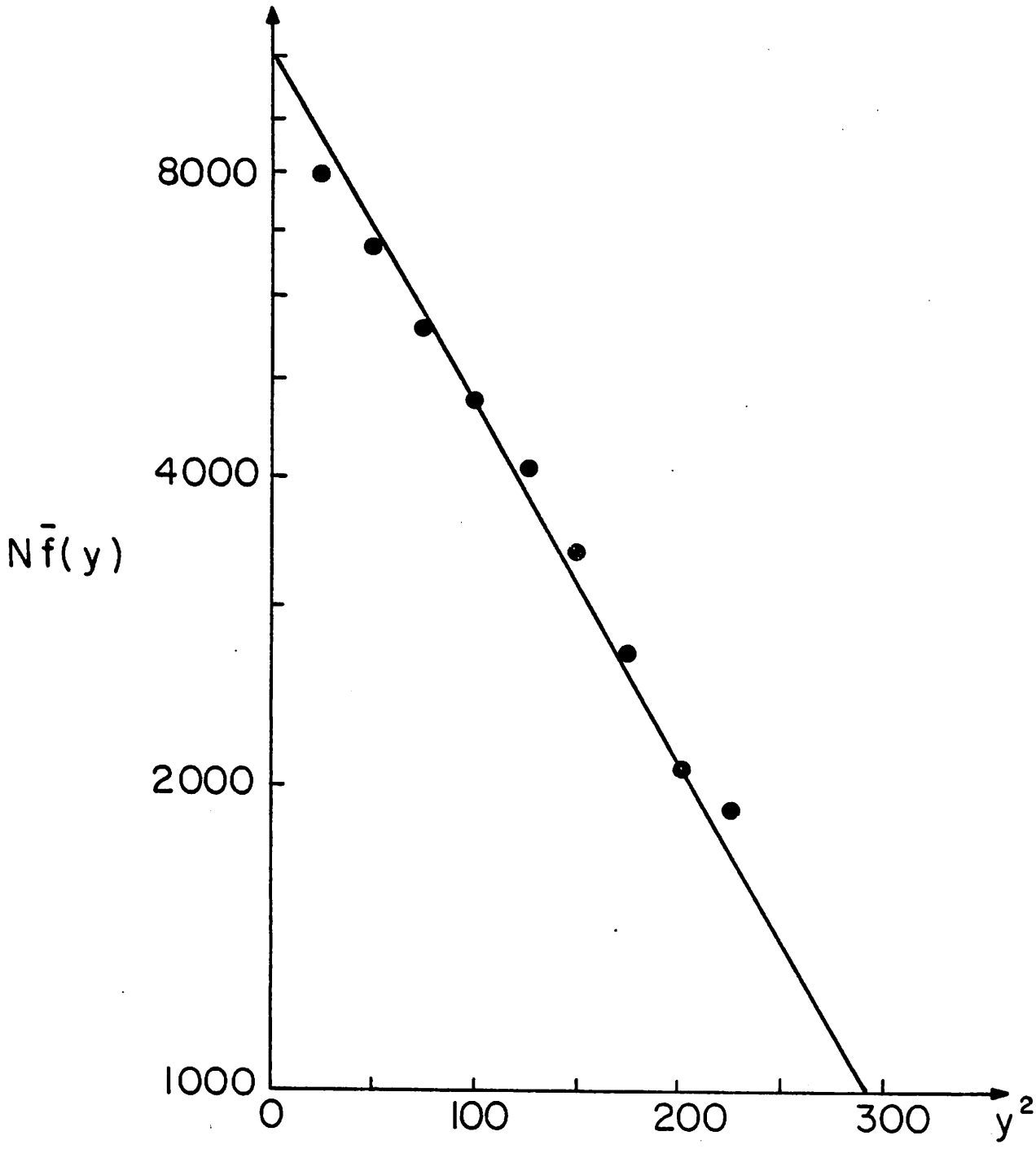

Fig. 7. Comparison of the numerically calculated phase-averaged invariant distribution with the Fokker-Planck solution $\bar{f}(y)$ for $\delta = 0.1$, $k = 5$, and $N = 10^6$ in the Zaslavskii map.

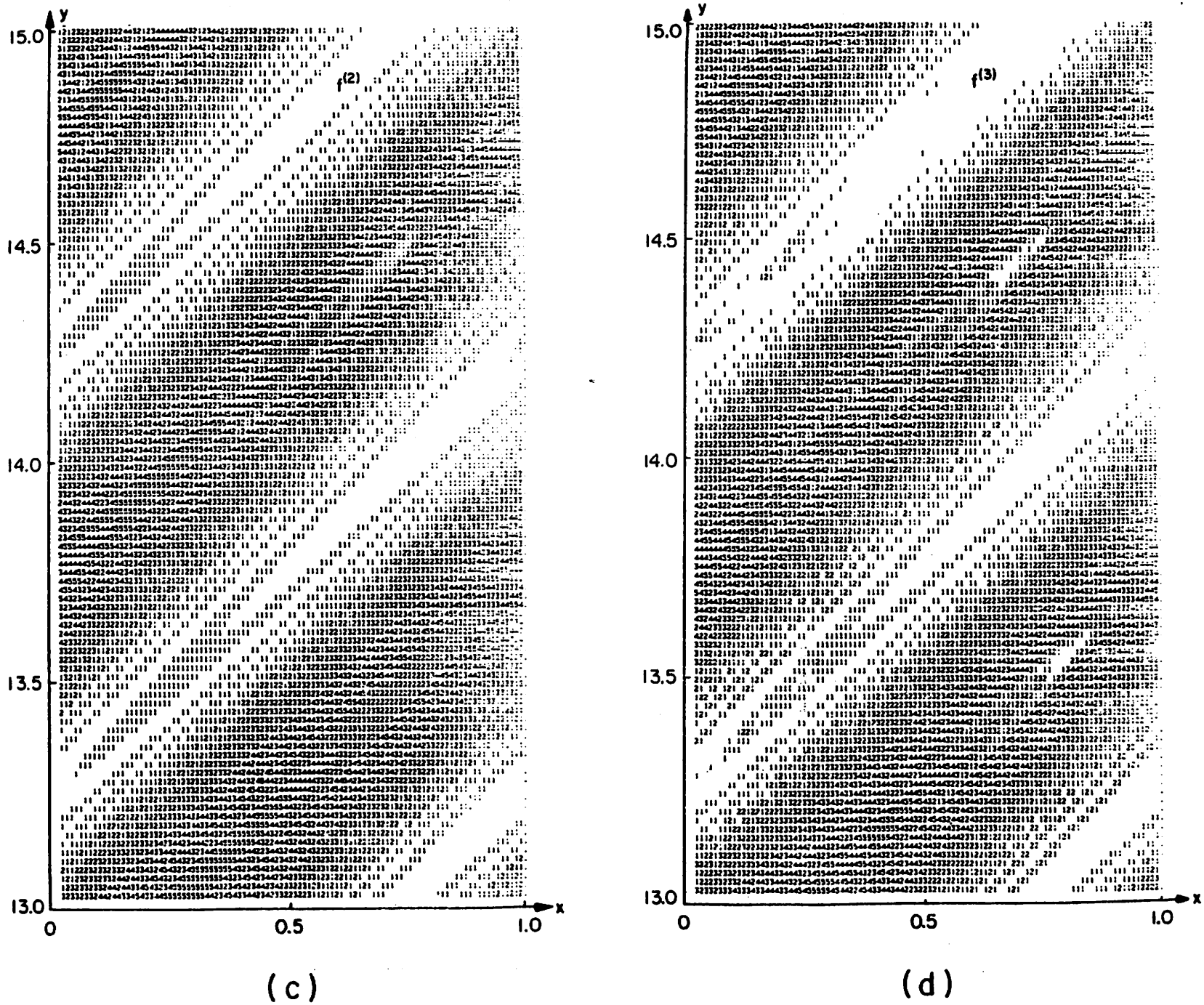

Fig. 8. Phase space y-x for the Zaslavskii map with $k = 5$ and $\delta = 0.1$, in the range $13 \leq y \leq 15$. (a) Numerically obtained from ten initial conditions having 100,000 collisions each. There are 23641 occupations shown. (b) Analytically obtained first order result $f^{(1)}(x,y)$; (c) Analytically obtained second order result $f^{(2)}(x,y)$; (d) Analytically obtained third order result $f^{(3)}(x,y)$.

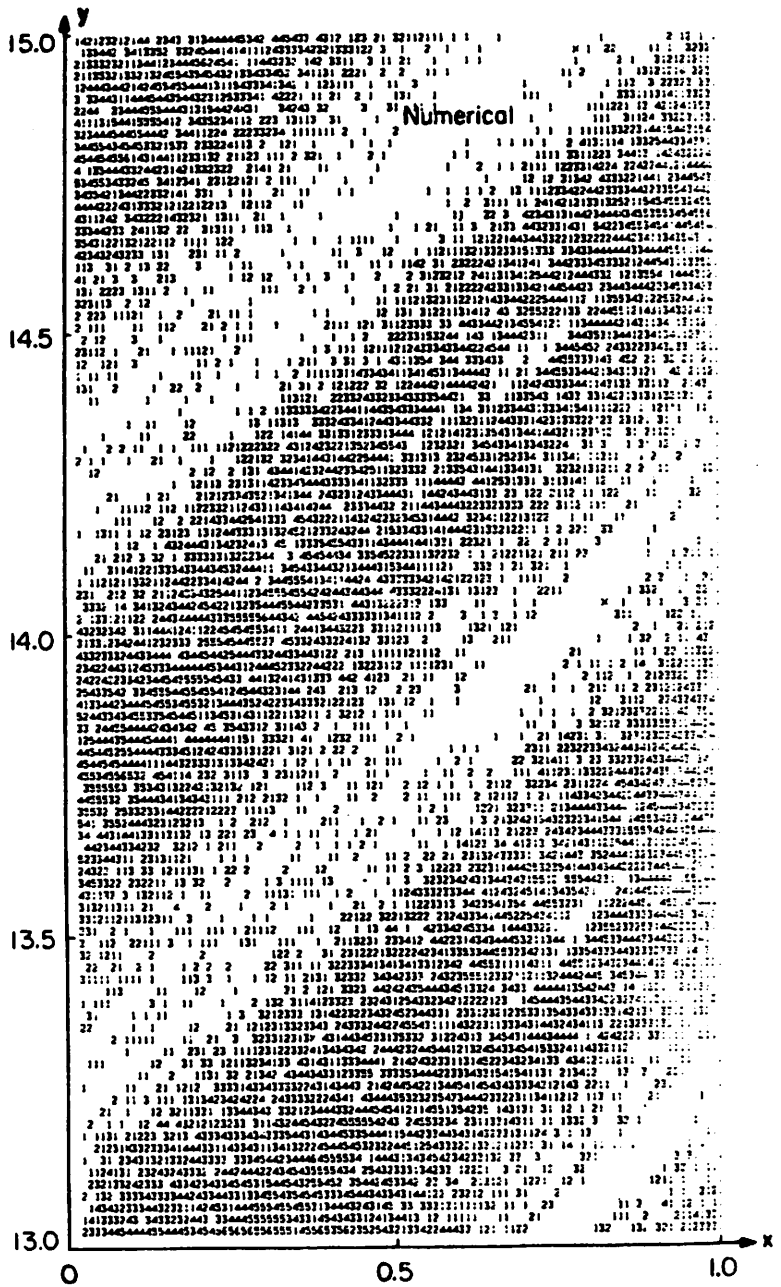
y
15.0
14.5
14.0
13.5
13.0
x
0
0.5
1.0
Numerical

(a)

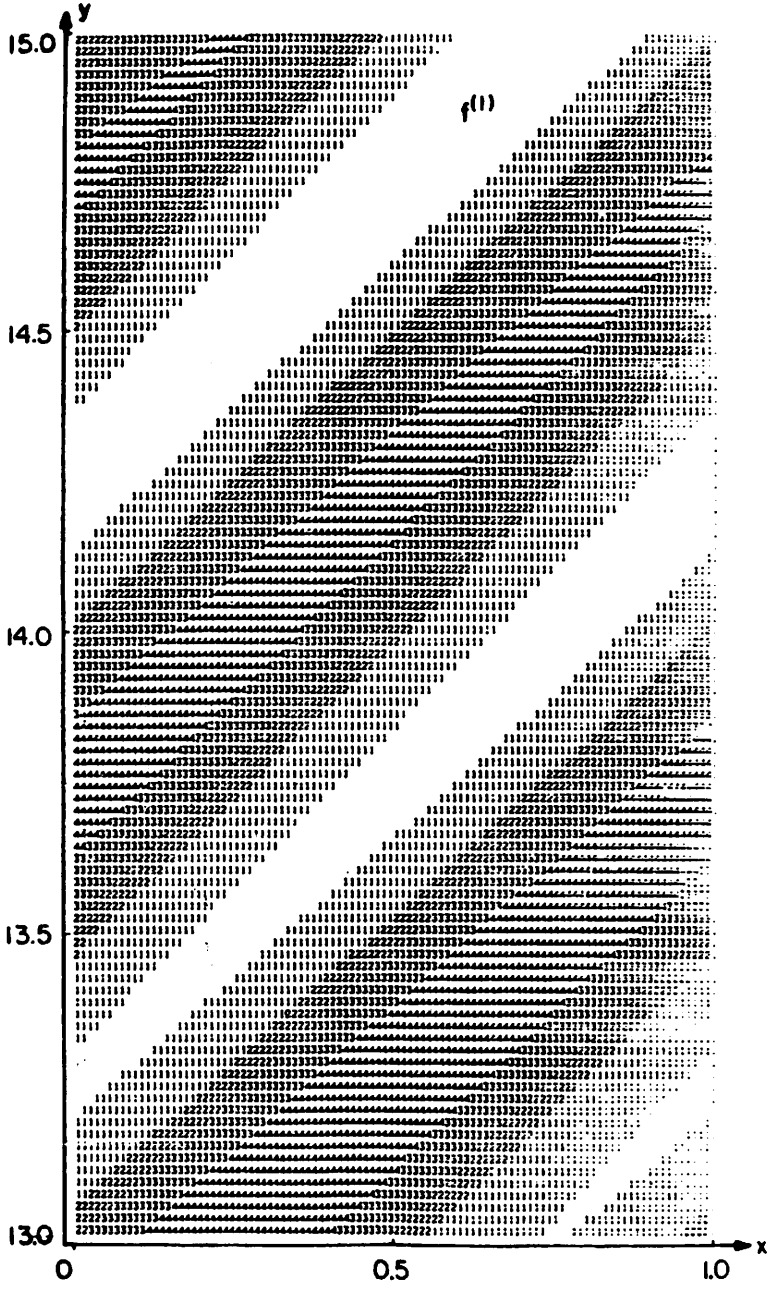
y
15.0
14.5
14.0
13.5
13.0
x
0
0.5
1.0
f(1)

(b)

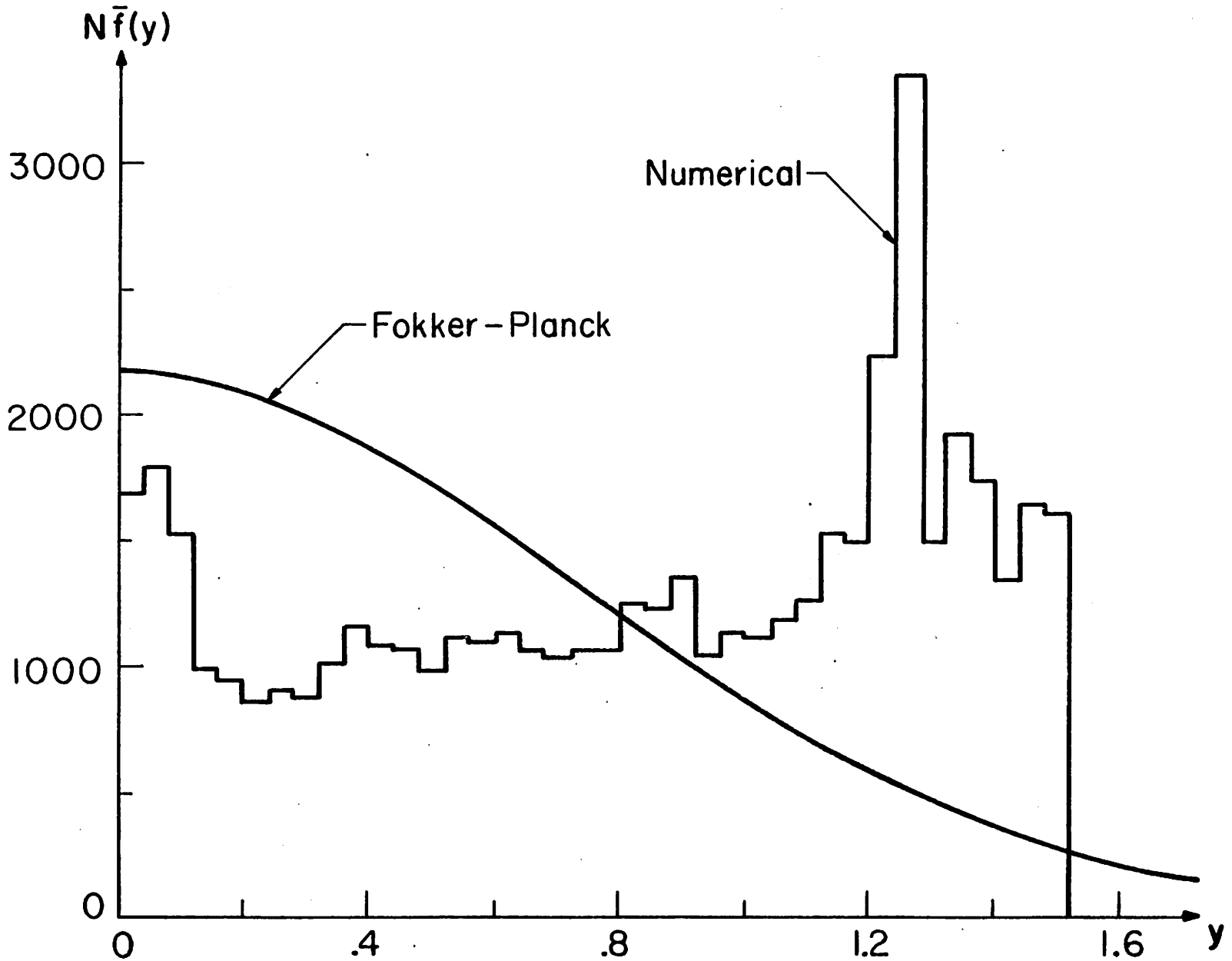

Fig. 9. Comparison of analytical and numerical phase-averaged distributions for the Zaslavskii map with $k = 1.4$, $\delta = 0.9$, and $N = 10^5$.

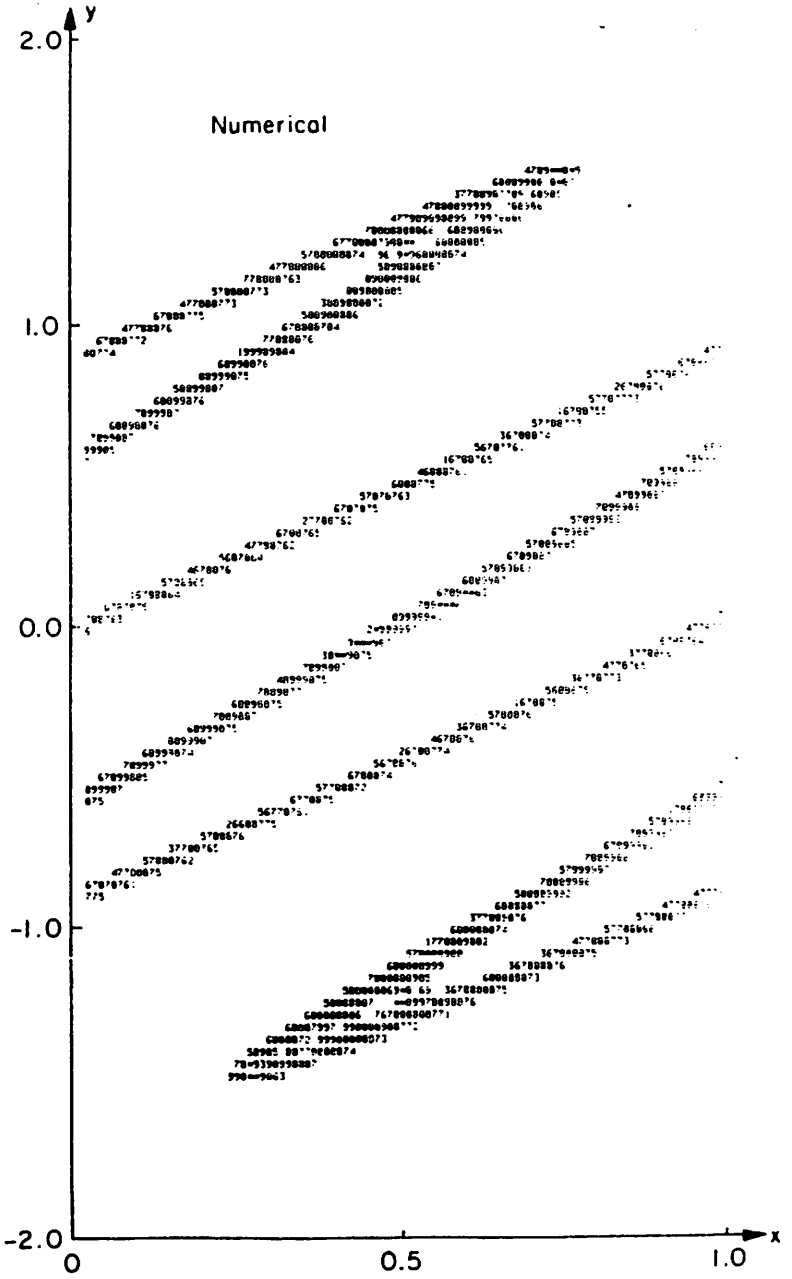

Fig. 10. Phase space y-x for the Zaslavskii map with $k = 1.4$ and $\delta = 0.9$, in the range $-2 \leq y \leq 2$. (a) Numerically obtained from one initial condition with 100,000 collisions; (b) Analytically obtained first order result $f^{(1)}(x,y)$; (c) Analytically obtained second order result $f^{(2)}(x,y)$.

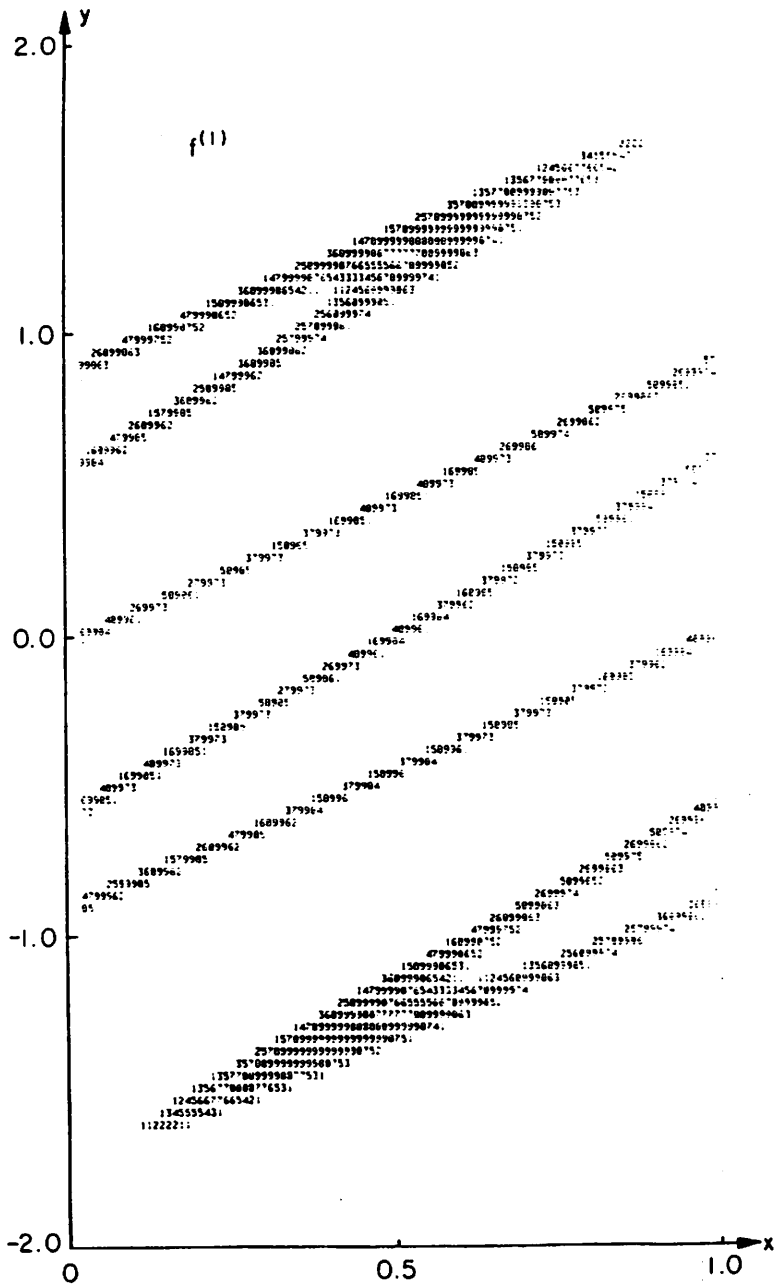

(b)

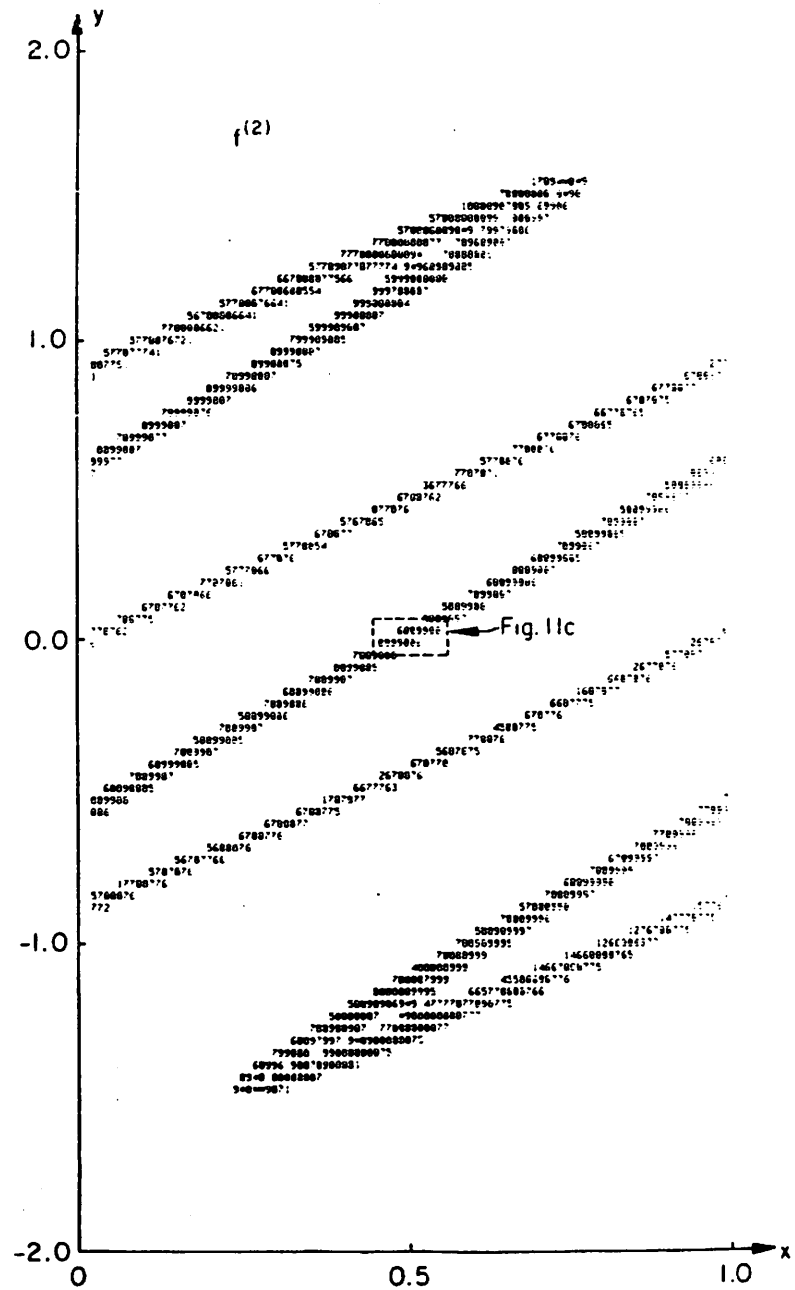

(c)

Fig. 10

Fig. 11.

Phase space y-x for the Zaslavskii map with $k = 1.4$ and $\delta = 0.9$, in the range $0.44 \leq x \leq 0.56$, $-.06 \leq y \leq .06$. (a) Numerically obtained from one initial condition with 1,000,000 collisions, of which 37326 occupations are shown; (b) Numerically obtained from ten initial conditions, each with 100,000 collisions; there are 37502 occupations shown; (c) Analytically obtained second order result $f^{(2)}(x,y)$.

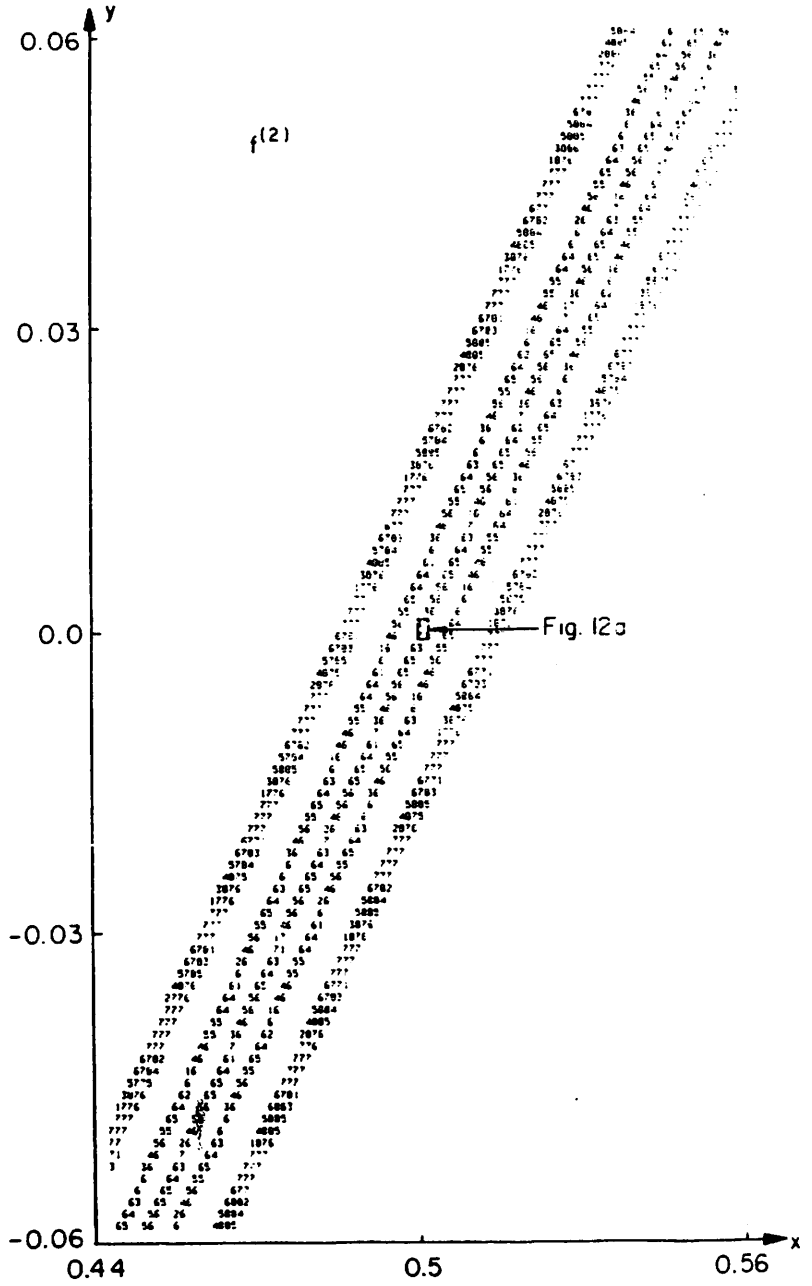

(c)

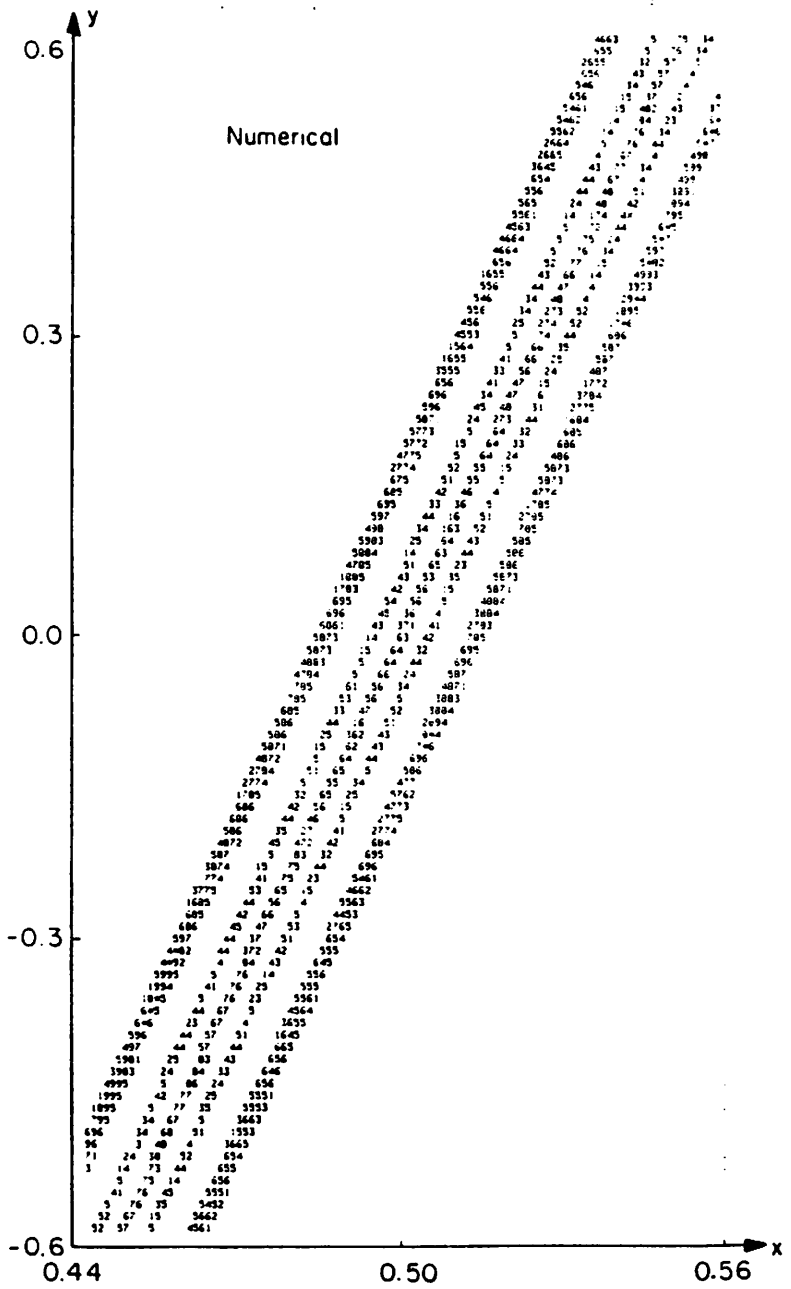
Numerical
y
x
0.6
0.3
0.0
-0.3
-0.6
0.44
0.50
0.56

(a)

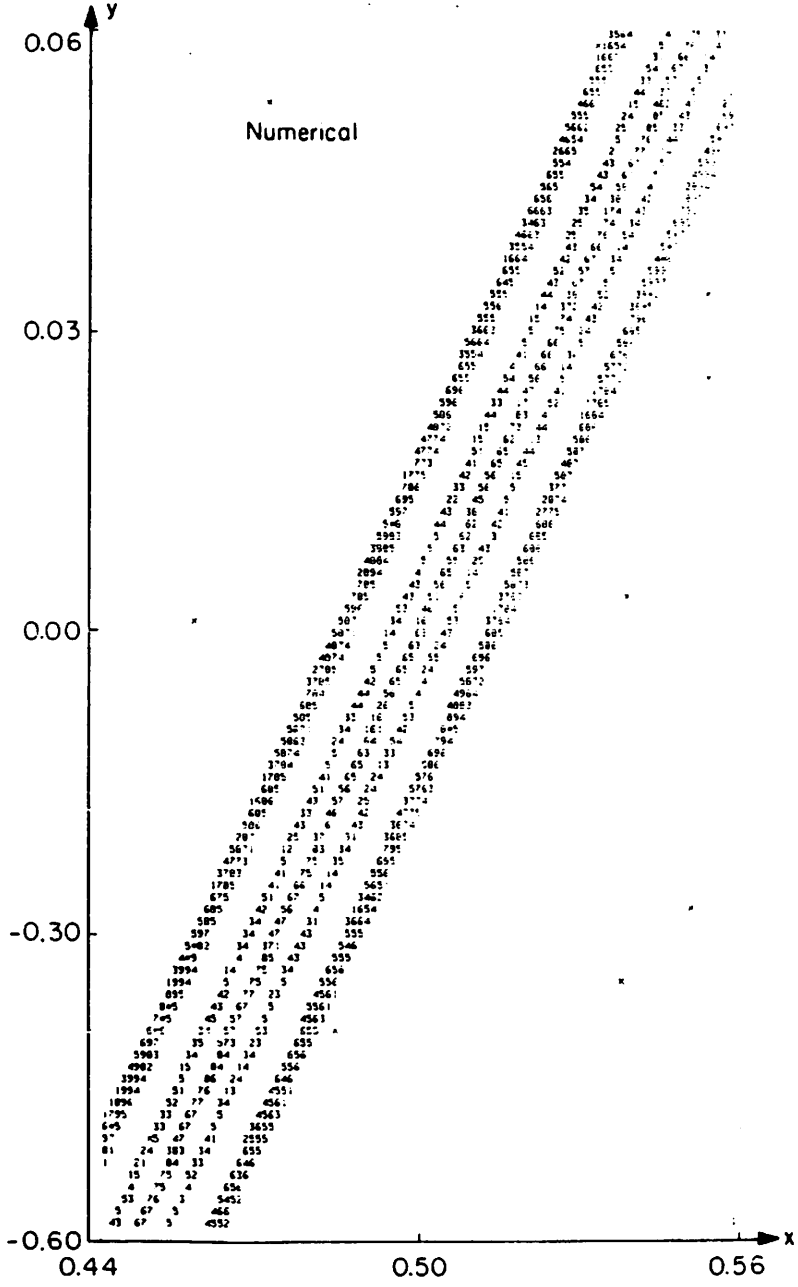
Numerical
y
x
0.06
0.03
0.00
-0.30
-0.60
0.44
0.50
0.56

(b)

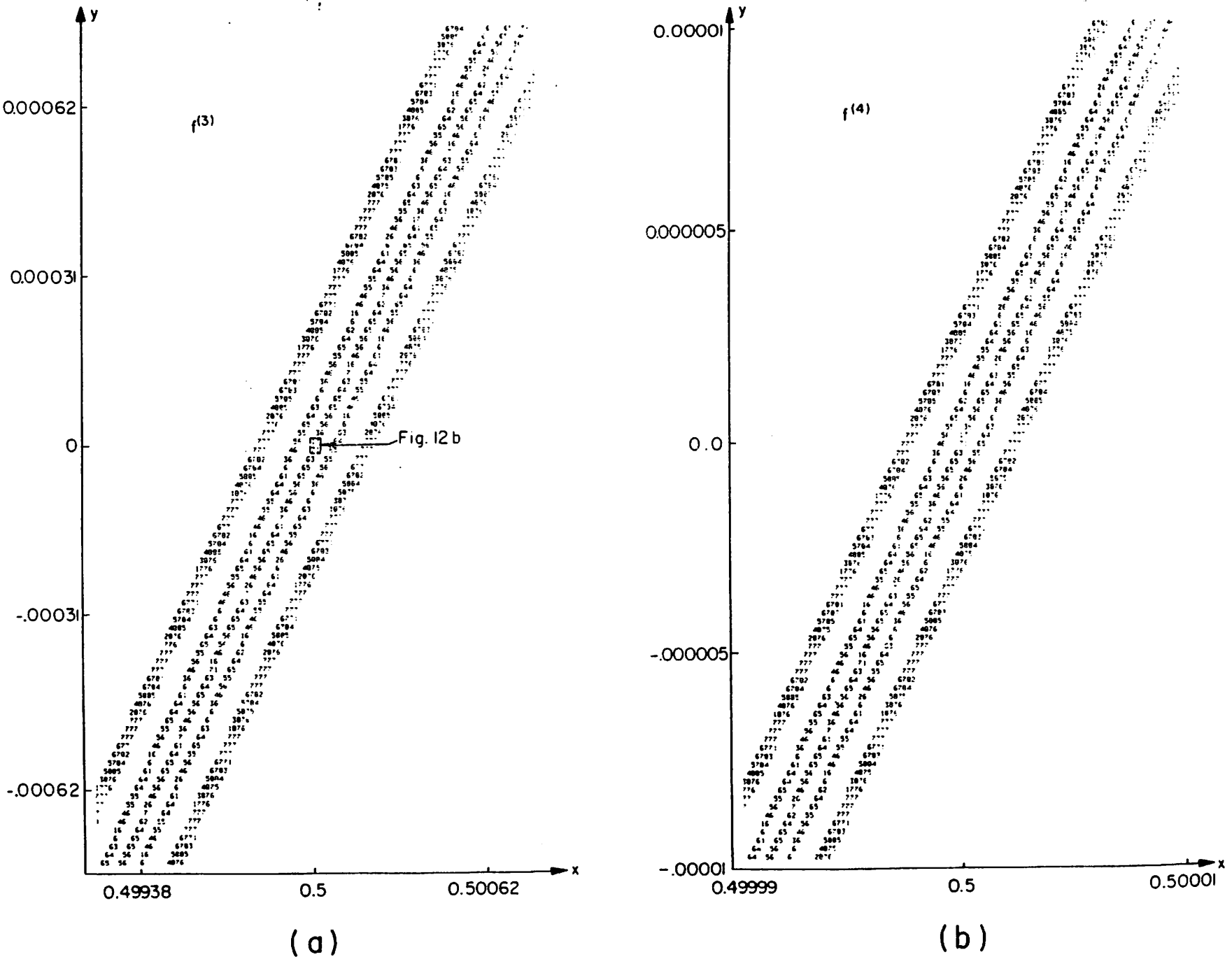

Fig. 12. Successive magnifications of the analytical result in Fig. 11c showing (a) third order structure and (b) fourth order structure.

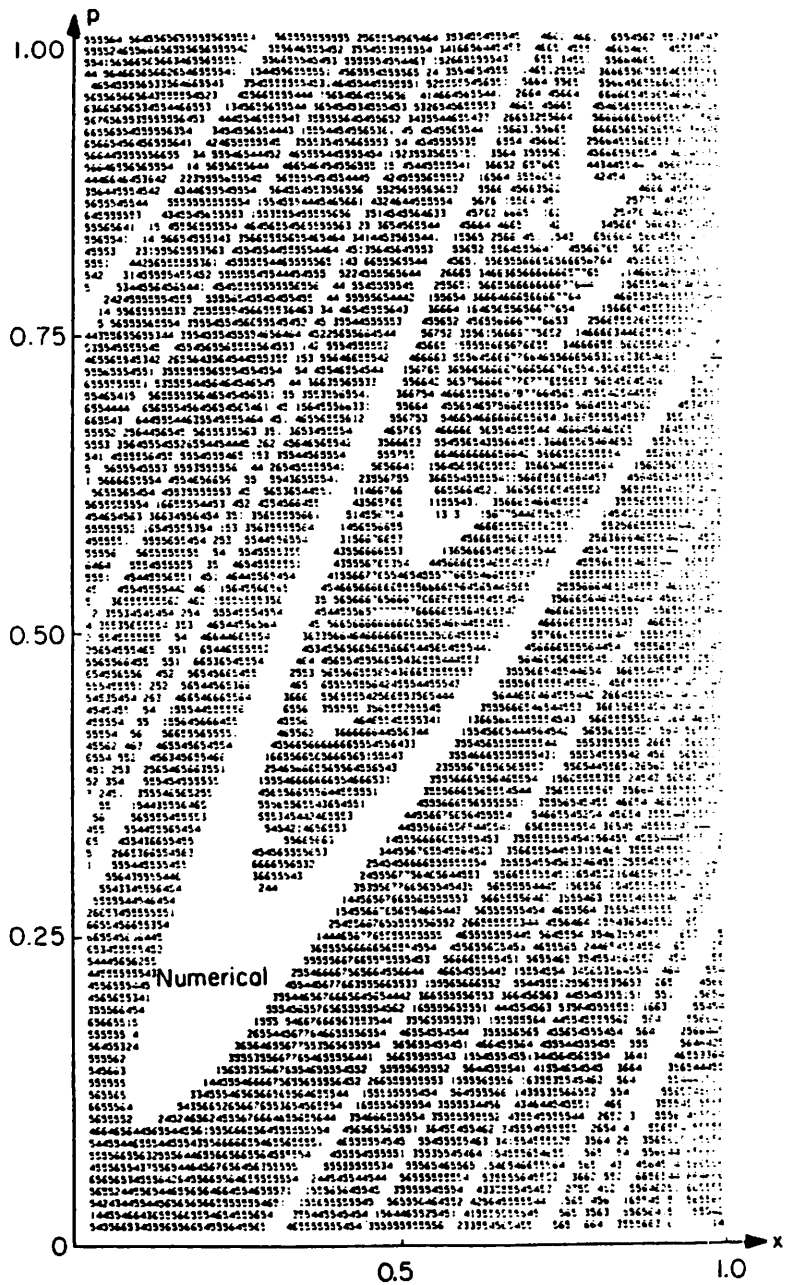

(a)

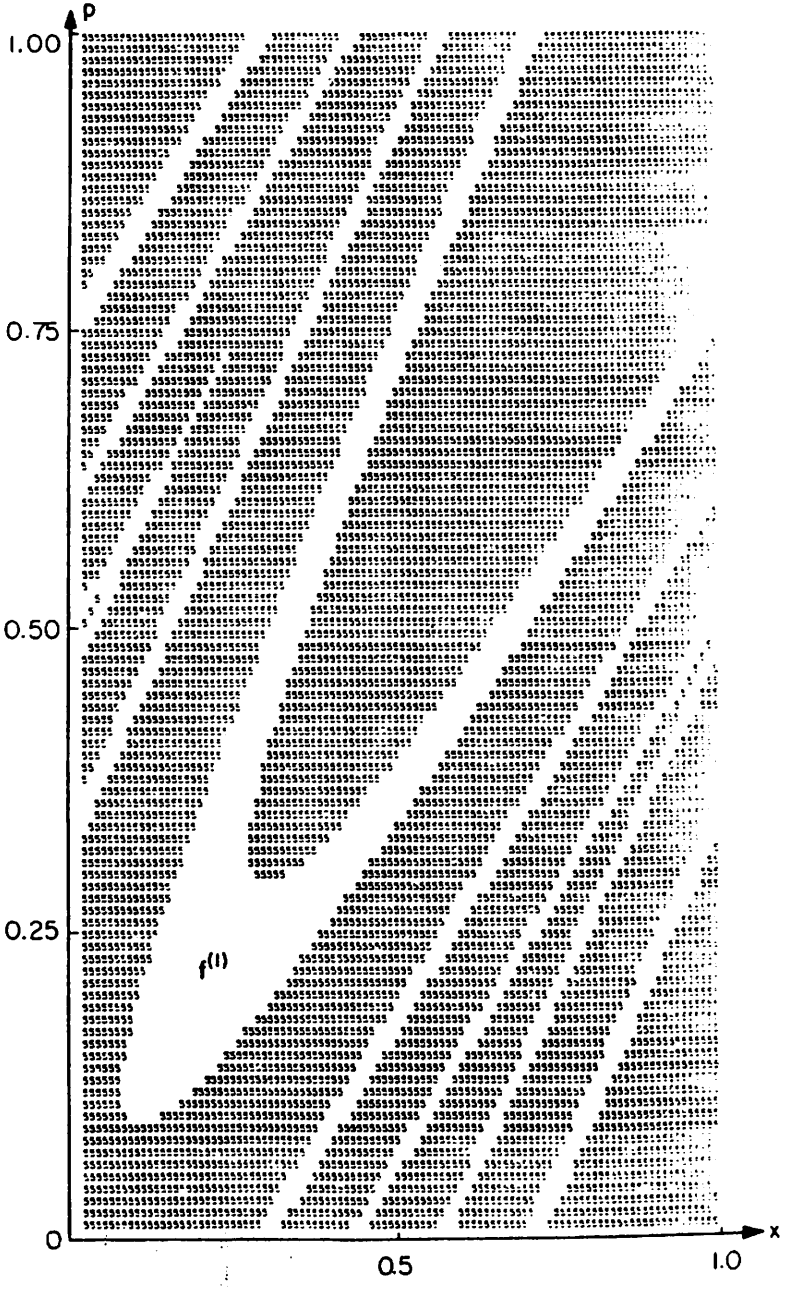

(b)

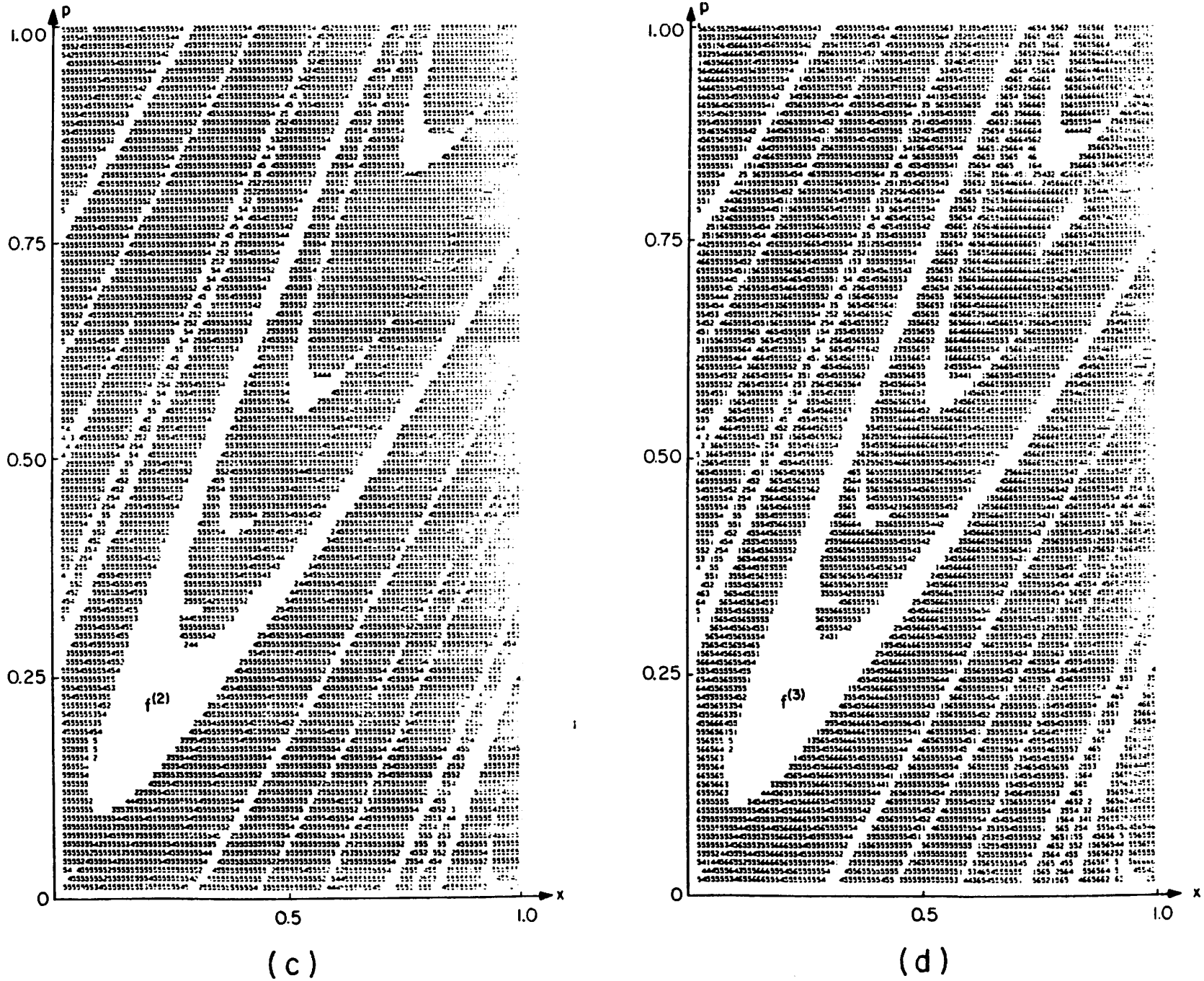

Fig. 13. Phase space p-x for the quadratic Chirikov mpa with $k = 9.76$ and $\delta = 0.2$ in the unit square. (a) Numerically obtained from one initial condition with 100,000 collisions; (b) Analytically obtained first order result $f^{(1)}(x,p)$; (c) Analytically obtained second reder result $f^{(2)}(x,p)$; (d) Analytically obtained third order result $f^{(3)}(x,p)$.